Sufficient Conditions for Global Minimality of Metastable States in a Class of Non-Convex Functionals: a Simple Approach via Quadratic Lower Bounds

David Shirokoff[*]   Rustum Choksi[†]   Jean-Christophe Nave[‡]

February 6, 2015

Abstract

We consider mass-constrained minimizers for a class of non-convex energy functionals involving a double-well potential. Based upon global quadratic lower bounds to the energy, we introduce a simple strategy to find sufficient conditions on a given critical point (metastable state) to be a global minimizer. We show that this strategy works well for the one exact and known metastable state: the constant state. In doing so, we numerically derive an almost optimal lower bound for both the order-disorder transition curve of the Ohta-Kawasaki energy and the liquid-solid interface of the Phase-Field Crystal energy. We discuss how this strategy extends to non-constant computed metastable states, and the resulting symmetry issues which one must overcome. We give a preliminary analysis of these symmetry issues by addressing the global optimality of a computed lamellar structure for the Ohta-Kawasaki energy in one (1D) and two (2D) space dimensions. We also consider global optimality of a non-constant state for a spatially in-homogenous perturbation of the 2D Ohta-Kawasaki energy. Finally we use one of our simple quadratic lower bounds to rigorously prove that for certain values of the Ohta-Kawasaki parameter and aspect ratio of an asymmetric torus, any global minimizer $v(x)$ for the 1D problem is automatically a global minimizer for the 2D problem on the asymmetric torus.

Keywords: Global minimizers, non-convex energy, double-well potential, metastable state, convex/quadratic lower bound, Ohta-Kawasaki functional, phase-field crystal functional.

AMS Subject Classifications: 49M30, 49S05.

1   Introduction

Pattern formation in complex systems (both physical and biological) has attracted much attention in applied mathematics and condensed matter physics. A classical viewpoint, emerging from ideas of Turing, has been that pattern formation outside of thermal equilibrium can be

---

[*]Dept. of Mathematical Sciences, NJIT, Newark, NJ, USA, david.g.shirokoff@njit.edu

[†]Dept. of Mathematics and Statistics, McGill University, Montreal, Canada, rchoksi@math.mcgill.ca

[‡]Dept. of Mathematics and Statistics, McGill University, Montreal, Canada, jcnave@math.mcgill.ca

captured via bifurcations off a homogeneous (thermal equilibrium) state, wherein patterns are classified according to linear instabilities of the homogeneous state (cf. [9]). On the other hand, in systems which are driven out of thermal equilibrium it is often the case that there is some non-convex energy functional associated with the phenomenon, and the PDE models used are indeed variational; that is, they represent a gradient flow (with respect to some metric) of a postulated "energy". We call such systems **energy-driven**, and often periodic pattern formation is a direct consequence of the competition between different terms in the energy [22, 16].

In this article, we address a ubiquitous class of non-convex functionals associated with energy-driven pattern formation, focusing on two paradigms: the Ohta-Kawasaki energy [20] used to model self-assembly of diblock copolymers, and a variant of the Swift-Hohenberg energy [23, 9, 12] used in phase-field crystal modeling. These functionals and the associated variational problems are defined for order parameters u with fixed relative average $m \in (-1, 1)$ (conserved "mass"). They share the following common features:

- They are based upon a double-well potential regularized with higher order terms. As such they may be viewed as offsprings of the ubiquitous Ginzburg-Landau functional. The wells represent two preferred states (*phases*) of the order parameter u. Energetically, the additive regularization prefers pure phases – regions of space wherein u is essentially constant.

- They also contain a term which *competes energetically* with the regularization, favoring modulations (oscillations) of the order parameter u. This competition is responsible for periodic pattern formation, that is, minimizers tend to be periodic on an intrinsic scale. In addition to the mass parameter m, a parameter denoted here by γ (or ϵ) weighs the relative importance of the different terms. Together, these two parameters control the pattern morphology of minimizers.

- The constant state $u \equiv m$ remains a critical point for all values of γ (resp. ϵ).

- For most points in the γ (resp. ϵ) vs. m phase plane, the associated energy landscape is **highly non-convex** with a tremendous number of critical points and local minimizers around which the energy landscape is relatively **"flat"**.

This last feature presents many difficulties in computing local and global minimizers. In particular, a gradient flow starting from any given state (for example, a random state) may appear to converge to a state which is not a local minimizer. Using gradient dynamics alone, one cannot distinguish between stable and unstable critical points, since they are both identified as solutions for which the relative change in the order parameter or the energy between time-steps is smaller than some tolerance level. We call such states **metastable**. These include states which are sufficiently "near" to local minimizers that the gradient dynamics are so slow that solutions appear to be stable. This sort of *dynamic metastability* can be misleading in the sense that after a long time, the solution undergoes drastic change. Techniques for dealing with metastability and highly non-convex energy landscapes often belong to the broad class of statistical methods which include techniques of *simulated annealing*. They were created to navigate through a complex energy landscape, surpassing energy *barriers* in search of a global minimizer. An example of such a technique is spectral weighting or spectral projection ([5]).
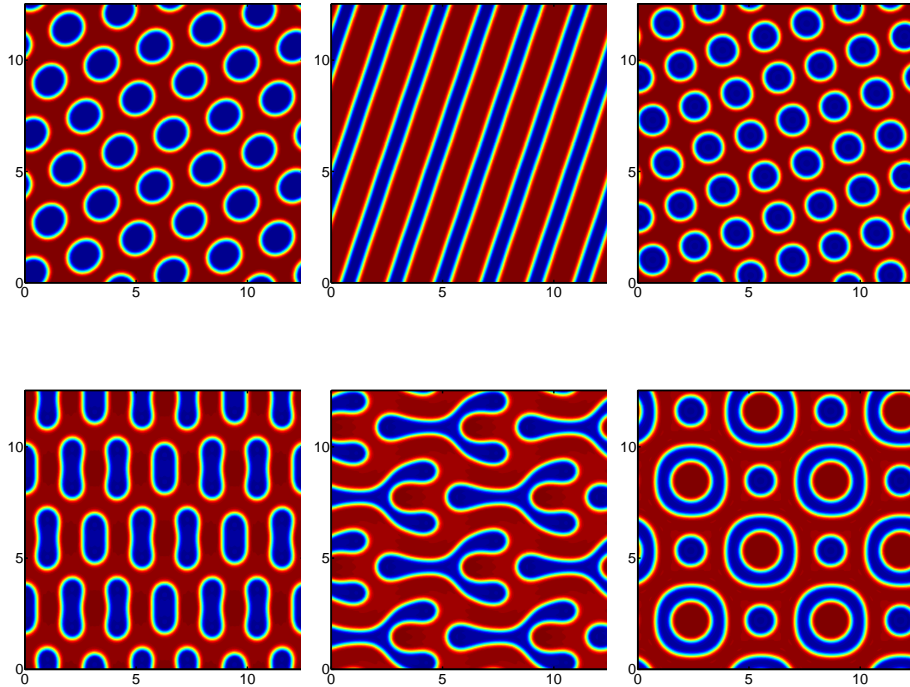
2

Figure 1: Metastable states associated with the gradient flow of the Ohta-Kawasaki (**OK**) functional with $m = 0.25, \gamma = 10$. The first result (hexagonally packed spots) has the lowest energy per unit area and we believe it represents a depiction of the ground state. The energy densities of the states are (l-r) top row $0.1218, 0.1234, 0.1263$ and bottom row $0.1239, 0.1263, 0.1265$.

This technique is used in Figure 1 to show the vast array of metastable states. They show final metastable states for simulations of the H^{-1} gradient flow of the (**OK**) functional with $m = 0.25, \gamma = 10$. In each case, we start with random initial data but use several iterations of spectral projection to push the flow into a metastable state. Figure 2 shows another metastable state resulting from straight gradient flow with random initial conditions. While this structure exhibits defects and a lack of symmetry, it is not clear as to the type of metastable state, e.g. dynamically metastable or local minimizer. Note that the hexagonally packed spots in Figure 1 have the lowest energy per unit area and we believe this represents a depiction of the ground state.

Clearly if one wants to address the energy landscape of a non-convex functional with a goal of describing global minimizers throughout the phase plane, *neither* the local analysis around critical points, *nor* the solution of a gradient flow from any given state, is sufficient. Moreover, in contrast to 2D pattern formation where simple stripes and spots form the basis of the overriding patterns, the analogous class of metastable and minimizing patterns in 3D is far more complex, and any sort of classification is as yet unclear. Thus, studying 3D pattern formation from purely the PDE point of view is unproductive without guidance from the overall
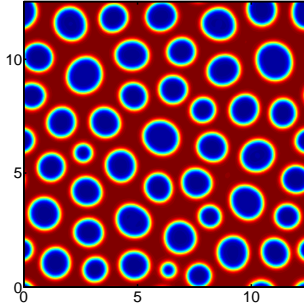
Figure 2: A metastable state obtained by running a gradient flow starting with random initial conditions. Here $m = 0.25, \gamma = 10$ while the relatively high energy density is 0.1290. Note that the state exhibits defects and a lack of symmetry.

energy landscape. A long term goal is to *exploit the structure of the energy functional* to

- develop verification strategies (based upon sufficient conditions) for determining whether or not a computed steady state is a global minimizer;

- develop and explore tools of *simulated annealing* for navigating through the non-convex energy landscape in order to access low energy states.

In this article, we focus on the first goal by deriving global quadratic lower bounds to the energy about a given metastable state. In Section 3, we consider the simplest, so-called disordered, state associated with a constant order parameter. For any fixed m, when γ (resp. ϵ) is sufficiently small, the constant state $u \equiv m$ becomes energetically favorable. We derive a new strategy to determine when the disordered state is the (unique) global minimizer. More precisely, we find a lower bound on the order-disorder curve (ODT) in the phase plane which is simply the curve below which the disordered state is the unique global minimizer. Note that a standard (local) technique pertaining to the ODT (or in fact any phase transition) is via linear stability analysis ([9]). Linear stability analysis about the constant state gives an *upper bound* on the true ODT, since above the linear stability curve the constant state is linearly unstable and hence cannot possibly be a minimizer. From the point of view of global minimization this gives little information. What does give precise information, and requires a different argument, is a *lower bound* on the ODT; this is our strategy here. It is simple and based upon a very common theme in the modern calculus of variations: Replace a non-convex variational problem with an "suitable" convex problem which one can solve. In Sections 4 and 5, we discuss how this strategy can be used to find sufficient conditions on non-constant computed metastable states to be global minimizers.

Let us give a few details about our simple strategy. As we explain in the next section, the class of non-convex variational problems considered here all take the form: Minimize

$$\mathcal{F}[u] = a(u, u) + \int_\Omega \frac{1}{4}(1 - u^2)^2 \, \mathrm{d}\mathbf{x},$$

4

over all u with average m in some Sobolev space. Here, a denotes a bilinear form on the Sobolev space. We are interested in verifying whether a given critical point v is a global minimizer of $\mathcal{F}$. This amounts to showing

$$\mathcal{F}[v + f] - \mathcal{F}[v] \geq 0, \qquad \forall f \in \mathcal{H},$$

where $\mathcal{H}$ is the subspace of mean zero functions in the Sobolev Space. Using the fact that v is a critical point, i.e., vanishing first variation in the sense of (4.2), we have

$$\mathcal{F}[v + f] - \mathcal{F}[v] = a(f, f) + \int_\Omega \left(\frac{3v^2}{2} - \frac{1}{2} \right) f^2 + vf^3 + \frac{f^4}{4} \; d\mathbf{x}. \qquad (1.1)$$

Using the structure of $\mathcal{F}$, we now attempt to bound from below the right hand side by a convex quadratic functional $Q[f] = Q(f, f)$[1]. Then if the quadratic bilinear form Q is positive semi-definite, i.e., for some $C \geq 0$

$$Q(f, f) \geq C \int_\Omega f^2 dx,$$

then v will be the global minimizer for the particular choice of parameters γ (resp. ϵ) and m. Note that a, and hence Q and the constant C, will depend on these parameters, and moreover, Q will also depend on v. Thus, sufficient conditions for global minimality are transferred to linear conditions based upon the positivity of the eigenvalues of an associated linear operator on $\mathcal{H}$. Both the structure of v and the energy functional $\mathcal{F}$ will be used deriving the lower bound Q. We present two approaches:

1. The first approach is particularly simple and based upon elementary inequalities (e.g. the Cauchy-Schwarz inequality in the L^2 sense).

2. The second approach uses more information about the functional by invoking the Cauchy-Schwarz inequality in the inner product induced by the second variation bilinear form (a together with the quadratic terms in (1.1)).

These approaches allow us to numerically compute values for C.

As we show in Section 3, this strategy works very well for the simplest critical point, the constant state $v \equiv m$. The constant state is indeed special as it remains a critical point throughout the entire phase plane, moreover it is stable throughout a region of the phase plane. In Section 4 and 5 we specialize to the Ohta-Kawasaki functional and address non-constant critical points. Non-constant states are particularly important as rigorous results about global minimizers for these are scarce (cf. [4] and the references therein). On the torus, the energy is invariant under certain symmetry transformations, and this results in degeneracy issues for our lower bounds. These issues require one to constrain the set of possible perturbation functions f. In Section 4.3, we argue that a computed lamellar state in 1D is nearly optimal. In Section 4.4, we computed a lamellar state in 2D, but at present, give only a partial picture as a result

---

[1] Given the simplicity of the idea of a global convex bound, it seems likely that it has been invoked in the past. We note that the idea has been recently used in [11] to study profiles of point defects in the Landau-de Gennes theory of liquid crystals.

of the larger number of symmetry transformations. However, by working on an asymmetric rectangular torus, we show that our method is successful (Section 4.5). In Section 4.6, we address global optimality of a computed metastable state for a perturbed functional which includes a spatially non-symmetric potential. In Section 5, we use our first lower bound to rigorously prove that for certain values of the Ohta-Kawasaki parameter and aspect ratio of an asymmetric rectangular torus, any global minimizer $v(x)$ for the 1D problem on the torus is automatically a global minimizer for the 2D problem on the asymmetric 2D torus. Combining this with previous work [18, 21, 25] on minimizers in 1D, we obtain a proof of the existence of periodic, lamellar global minimizers on certain 2D domains.

Given that our strategy will reduce to linear analysis based upon a critical point, it is important to differentiate our analysis with standard local perturbation theory which is also based upon a linear operator about a critical point. Figure 3 illustrates the difference via a simple non-convex finite-dimensional energy (in black). Focusing on the critical point at $x = 0$, the top parabola (in blue) on the left illustrates the standard theory based upon the analysis of an approximating convex (parabolic) function which is locally a good "fit" at $x = 0$. On the other hand, the bottom parabola (in red) illustrates our approach based upon the analysis of a convex (parabolic) lower bound to the entire energy. For this finite-dimensional case, it is clear that one could simply choose the convex hull of the energy. In our infinite-dimensional setting, our strategy will be to find a "good" quadratic lower bound based upon information about the energy $\mathcal{F}$.
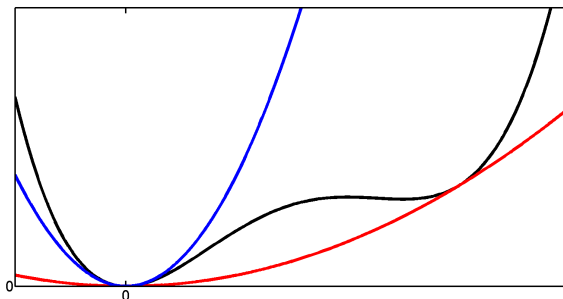

Figure 3: Simple schematic illustrating our approach vs. the standard local approach.

We end with a few important remarks concerning our focus on global minimizers[2]. For any physical application, one could certainly argue that the ground state is in fact not *accessible*, and hence have reservations for a study which is focused on its structure and how to reach it. Indeed, even if the *energy* has direct physical meaning most thermodynamical principles do not dictate global energy minimization. On the other hand, global energy minimization has often proved to be a *convenient* postulate for gaining insight into a variety of phenomena. In the current situation, without guidance from the energy one would have no way of weeding out "non-desirable" (non-physical) metastable states; this is particularly pertinent in 3D where

---

[2]We must acknowledge that there are interesting phenomena at the level of critical points to Swift-Hohenberg-type energies. Of particular interest here are *localized patterns* (see for example [2]). There is also work on localized patterns for the Ohta-Kawasaki energy ([14]).

the number and complexity of metastable states is considerably higher. Thus, even if a global minimizer is not the eventual goal, strategies for navigating the energy landscape to achieve states of lower energy are of fundamental importance, and any results or methods which give insight into the overall energy landscape should prove fruitful. Moreover, we remind the reader that while much work is concerned with the *dynamics to a metastable state* (cf. [10]), these notions of *dynamics* are based upon a gradient flow which is a priori not well-defined; in fact, a gradient flow involves a choice of a metric, and based upon notions of entropy dissipation, one can debate the appropriateness of using different metrics. While the L^2 metric is often used without question, it has recently been shown that the Wasserstein metric is a natural metric for the variational interpretation of many time-dependent PDEs (cf. [15, 1]). For our class of mass-constrained problems, it is convenient to compute the gradient in the Hilbert space H^{-1}. Physicists call this the *diffusive dynamics*. For certain problems, e.g. the standard Cahn-Hilliard problem, the H^{-1} dynamics can be directly justified on purely physical grounds [3]. However, for other problems, for example the Ohta-Kawasaki energy, no such justification exists.

2   The Common Structure of the Energy Functionals

We begin with some notation. Throughout this article, Ω denotes a flat torus in $\mathbb{R}^n$ (usually $n = 2$ or 3). In other words, we invoke periodic boundary conditions throughout. We denote the average of any function ϕ on Ω by

$$\overline{\phi} := \fint_\Omega \phi(\mathbf{x}) \, \mathrm{d}\mathbf{x} = \frac{1}{|\Omega|} \int_\Omega \phi(\mathbf{x}) \, \mathrm{d}\mathbf{x}.$$

When we do not average we use the notation

$$\langle \phi \rangle := \int_\Omega \phi(\mathbf{x}) \, \mathrm{d}\mathbf{x}.$$

We denote the L^2 inner product and norm of functions u and v in $L^2(\Omega)$ by

$$\langle u, v \rangle := \int_\Omega u(\mathbf{x}) v(\mathbf{x}) \, \mathrm{d}\mathbf{x}, \qquad \|u\| := \langle u, u \rangle.$$

Our functionals will be defined over functions in the Sobolev Space $H^k(\Omega)$, $k = 1, 2$ with fixed average. The choice of k depends on the precise functional with $k = 1$ and 2 respectively for the Ohta-Kawasaki and Phase-Field Crystal functionals. Perturbation functions will have mean zero, and hence we will often work in the Hilbert space

$$\mathcal{H} := \left\{ f \in H^k(\Omega) \,\middle|\, \overline{f} = 0 \right\}, \quad \text{with either } k = 1 \text{ or } k = 2.$$

We will also use a version of the H^{-1} norm on functions in $L^2(\Omega)$ with mean zero. To this end, if $u \in L^2(\Omega)$ with $\langle u \rangle = 0$, then we define

$$\|u\|_{H^{-1}(\Omega)}^2 := \|\nabla(-\triangle)^{-1} u\|^2.$$

That is,

$$\|u\|^2_{H^{-1}(\Omega)} = \int_\Omega |\nabla v^2|\, d\mathbf{x} \qquad \text{where} \quad -\triangle v = u \text{ in } \Omega.$$

Note that this norm is simply the dual norm to H^1 with respect to the L^2 pairing. That is,

$$\|u\|_{H^{-1}(\Omega)} = \sup_{v \in H^1(\Omega)} \frac{\langle u, v \rangle}{\|\nabla v\|_{L^2(\Omega)}}. \tag{2.1}$$

We consider functionals of the following form:

$$\mathcal{F}[u] = a(u, u) + \int_\Omega \frac{1}{4}(1 - u^2)^2\, d\mathbf{x} \tag{2.2}$$

defined over functions $u \in H^k(\Omega)$ with average $\bar{u} = m$, for some fixed $-1 < m < 1$. Since a constant plays no role in the minimization, we can equivalently write (2.2) as

$$\mathcal{F}[u] = a(u, u) + \int_\Omega \frac{u^4}{4} - \frac{u^2}{2}\, d\mathbf{x}. \tag{2.3}$$

Here a represents a bilinear form on $H^k(\Omega)$, for some appropriate choice of $k \geq 1$. Functionals (2.2) arise in different physical problems, for example, in phase transitions in complex fluids, self-assembly of block copolymers, superconductivity, etc. Two specific examples are an appropriately rescaled version of the Ohta-Kawasaki functional for self-assembly of diblock copolymers (see [20, 6]) and a variant of the Swift-Hohenberg energy [23].

- The **Ohta-Kawasaki functional**, defined over

$$\mathcal{H}_m := m + \mathcal{H} = \left\{ u \in H^1(\Omega)\, \Big|\, \bar{u} = m \right\},$$

is given by

$$(\mathbf{OK}) \qquad \mathcal{F}_1[u] := \int_\Omega \frac{1}{2}\gamma^{-2}|\nabla u|^2 + \frac{1}{2}|\nabla(-\Delta)^{-1}(u - m)|^2 + \frac{1}{4}(1 - u^2)^2\, d\mathbf{x}.$$

Note that

$$\int_\Omega |\nabla(-\Delta)^{-1}(u - m)|^2\, d\mathbf{x} = \int_\Omega |\nabla v|^2\, d\mathbf{x} \qquad \text{where} \qquad -\Delta v = u - m \text{ in } \Omega.$$

In this case, the associated bilinear form a in (2.2), defined over $\mathcal{H}_m$, is given by

$$a_1(u_1, u_2) = \int_\Omega \frac{1}{2}\gamma^{-2}\nabla u_1 \cdot \nabla u_2 + \frac{1}{2}\nabla w_1 \cdot \nabla w_2\, d\mathbf{x}, \tag{2.4}$$

with $-\Delta w_i = u_i - m$ in Ω.

8

- The **Phase-Field Crystal functional** is an example of a Swift-Hohenberg-type functional commonly used in models for pattern formation ([23, 9, 19, 24]). This particular variant[3] [12, 13] is the functional defined over

$$\mathcal{H}_m := m + \mathcal{H} = \left\{ u \in H^2(\Omega) \,\middle|\, \overline{u} = m \right\}$$

by

$$\textbf{(PFC)} \qquad \mathcal{F}_2[u] := \int_\Omega \frac{1}{2} u(q_0^2 + \Delta)^2 u + \frac{1}{2}(1 - \epsilon)u^2 + \frac{1}{4}(1 - u^2)^2 \, \mathrm{d}\mathbf{x}.$$

For **(PFC)** the associated bilinear form in (2.2) is

$$a_2(u_1, u_2) = \int_\Omega \frac{1}{2}(q_0^2 + \Delta)u_1 \, (q_0^2 + \Delta)u_2 + \frac{1}{2}(1 - \epsilon)u_1 u_2 \, \mathrm{d}\mathbf{x}.$$

In what follows, we set $q_0 = 1$.

In all these functionals, the order parameter u describes an average material density and satisfies a fixed mass (or mass ratio) constraint: for a fixed m with $-1 < m < 1$, $\overline{u} = m$. The parameters γ (resp. ϵ) and m describe material properties and determine the morphology (structure) of minimizing states. More precisely, they determine the morphology of the domains, wherein u takes on one of two preferred values, and their diffuse interfaces. These patterns have an intrinsic length. For **(OK)**, this intrinsic length is set by γ, and results from the minimization via competition of the Dirichlet energy regularization with the long-range interaction repulsive term $\int_\Omega |\nabla(-\Delta)^{-1}(u - m)|^2 \, \mathrm{d}\mathbf{x}$. For **(PFC)**, the intrinsic length is directly set by the parameter q_0, which we will henceforth set to be 1. By integrating by parts in $\mathcal{F}_2$, we find

$$\int_\Omega \frac{1}{2} u(1 + \Delta)^2 u \, \mathrm{d}\mathbf{x} = \int_\Omega \frac{u^2}{2} + \frac{|\Delta u|^2}{2} - |\nabla u|^2 \, \mathrm{d}\mathbf{x}.$$

Hence we see it is now the negative of the Dirichlet energy which favors modulations and competes with the regularization $|\Delta u|^2$.

3   Analysis for the Constant State and Lower Bounds on the ODT Curve

The order-disorder phase transition (ODT) occurs when there is a transition in the global minimizer of the functional from the disordered (i.e., no phase separation) state $u(\mathbf{x}) \equiv m$. The curve in the γ (or ϵ) vs. m plane differentiates two regimes; one wherein the global minimizer is $u(\mathbf{x}) \equiv m$ and one wherein it is some state $u(\mathbf{x}) \not\equiv m$ which typically exhibits some symmetric pattern. One standard approach for computing the ODT curve is through a linear stability

---

[3]This functional is also related to what is commonly called the Coleman-Mizel functional introduced in 1984 in the context of second-order materials, and then studied in [8]. An interesting asymptotic analysis of this functional appears in [7].

analysis about the state $u(\mathbf{x}) \equiv m$. In all these functionals, such a calculation overestimates the critical parameters γ_c and ϵ_c. For instance, when the disordered state becomes unstable, the function $u(\mathbf{x}) \equiv m$ is certainly not a global minimizer of the functional. In contrast, the state $u(\mathbf{x}) \equiv m$ may be stable, yet still not minimize the functional. In our approach, we compute a region in which $u(\mathbf{x}) \equiv m$ is guaranteed to be the global minimizer. We therefore underestimate the exact ODT via a lower bound. However, we provide numerical evidence that this underestimation is small.

We consider **finite** perturbations in $\mathcal{H}$ of the general energy $\mathcal{F}$ about the disordered state. That is, we define **the excess energy about the disordered state** $u \equiv m$ in direction $f \in \mathcal{H}$, to be $\delta_m \mathcal{F}$ where

$$
\begin{aligned}
\delta_m \mathcal{F}[f] \ &:= \ \mathcal{F}[m+f] - \mathcal{F}[m] \\
&= \ a(m+f, m+f) + \int_\Omega \frac{1}{4}(1-(m+f)^2)^2 - a(m,m) - \frac{1}{4}(1-m^2)^2 \, \mathrm{d}\mathbf{x} \\
&= \ a(f,f) + 2a(f,m) + \int_\Omega \frac{1}{4}(1-m^2-2mf-f^2)^2 - \frac{1}{4}(1-m^2)^2 \, \mathrm{d}\mathbf{x} \\
&= \ a(f,f) + \int_\Omega (m^3-m)f + \left(\frac{3}{2}m^2 - \frac{1}{2}\right)f^2 + mf^3 + \frac{f^4}{4} \, \mathrm{d}\mathbf{x} \\
&= \ a(f,f) + \int_\Omega \left(\frac{3m^2}{2} - \frac{1}{2}\right)f^2 + mf^3 + \frac{f^4}{4} \, \mathrm{d}\mathbf{x} \\
&= \ b(f,f) + \frac{1}{4}\langle f^4 \rangle + m\langle f^3 \rangle. \qquad\qquad\qquad\qquad\qquad (3.1)
\end{aligned}
$$

Note that the linear terms in f vanish as the constant state is a critical point (vanishing first variation) of the energy functional[4]. Here, we have incorporated the quadratic terms into a new bilinear form b defined on $\mathcal{H}$, i.e.,

$$
b(f,g) := a(f,g) + \int_\Omega \left(\frac{3m^2}{2} - \frac{1}{2}\right) f\, g \, \mathrm{d}\mathbf{x}. \qquad\qquad (3.2)
$$

The form $b(f,f)$ is none other than $1/2$ the *second variation* of the functional $\mathcal{F}$ about the critical point $u \equiv m$, taken in direction f. For (**OK**), this bilear form is

$$
b_1(f,g) := \int_\Omega \frac{1}{2}\gamma^{-2}\nabla f \cdot \nabla g + \frac{1}{2}\nabla w_1 \cdot \nabla w_2 + \frac{1}{2}(3m^2-1)fg \, \mathrm{d}\mathbf{x},
$$

where

$$
-\Delta w_1 = f \qquad \text{and} \qquad -\Delta w_2 = g.
$$

For (**PFC**) with $q_0 = 1$, the associated bilinear form is

$$
b_2(f,g) := \int_\Omega \frac{1}{2}[(1+\Delta)f]\,[(1+\Delta)g] + \frac{1}{2}(3m^2-\epsilon)fg \, \mathrm{d}\mathbf{x}.
$$

---

[4]For example, in (**OK**) the term $a(f,m) = 0$ trivially, while in (**PFC**) the term $a(f,m) = 0$ follows from $\langle f \rangle = 0$.

10

Our general strategy is to seek a quadratic functional $Q[f]$ defined on $\mathcal{H}$ such that

$$Q[0] = 0 \qquad \text{and} \qquad \delta_m \mathcal{F}[f] \geq Q[f] \ \text{ for all } \ f \in \mathcal{H}.$$

Then if in addition $Q[f]$ is positive semi-definite, i.e., $Q[f] \geq 0$ for all $f \in \mathcal{H}$, we are guaranteed that the disordered state $u(\mathbf{x}) \equiv m$ is a global minimizer of $\mathcal{F}[u]$.

Note that b depends on the parameters γ (resp. ϵ) and m, and we are seeking conditions for which $u(\mathbf{x}) \equiv m$ is a global minimizer. Hence without loss of generality, we work in the parameter regime of positive-definite second variation

$$b(f, f) > 0 \quad \text{for all} \quad f \neq 0. \tag{3.3}$$

We remark that this assumption may not in general hold when one analyzes a non-constant state as $b(f, f)$ may only be positive semi-definite across parameter space due to certain symmetry invariances of the energy. The degeneracy due to symmetry does not however effect the constant state.

We now use the trivial consequence of $(\alpha + \beta)^2 \geq 0$, that

$$\text{for } \alpha > 0 \text{ and any } \beta \qquad \alpha + 2\beta \geq -\frac{\beta^2}{\alpha}, \tag{3.4}$$

applied to

$$\alpha = \frac{1}{4}\langle f^4 \rangle \qquad \beta = \frac{m}{2}\langle f^3 \rangle,$$

to find from (3.1)

$$\delta_m \mathcal{F}[f] \ \geq \ b(f, f) - m^2 \frac{\langle f^3 \rangle^2}{\langle f^4 \rangle} \tag{3.5}$$

$$= \ b(f, f)\Big[1 - m^2 \frac{\langle f^3 \rangle^2}{b(f, f)\langle f^4 \rangle}\Big]. \tag{3.6}$$

In general, one can always rescale a function to saturate the inequality (3.5). Therefore, to describe the exact ODT curve, the critical parameters γ_c and ϵ_c must satisfy the following criteria

$$\max_f \frac{\langle f^3 \rangle^2}{b(f, f)\langle f^4 \rangle} = m^{-2}. \tag{3.7}$$

Solving (3.7) is difficult, essentially as difficult as the original problem. However, all is not lost as one can now replace (3.7) with an approximate convex problem. To this end, we will apply the Cauchy-Schwarz inequality to (3.6). We first do this with respect to the usual L^2 inner product and then show that we can produce a sharper lower bound by using the inner product induced by b. Note that by (3.3) and the fact that $b(f, g) = b(g, f)$ for all f, g, the quadratic functional $b(f, g)$ defines an inner product:

$$\langle f, g \rangle_b \ := \ 2b(f, g). \tag{3.8}$$

11

In addition, we can relate the inner product $\langle \cdot, \cdot \rangle_b$ to the conventional L^2 inner product by introducing the positive-definite, self-adjoint operator[5] B defined on $\mathcal{H}$ by

$$\langle f, g \rangle_b \quad =: \quad \langle f, Bg \rangle. \tag{3.9}$$

The operator B defined on $\mathcal{H}$ is invertible on $\mathcal{H}$.

3.1 First quadratic lower bound.

As a first attempt to find a quadratic lower bound on $\delta_m \mathcal{F}[f]$, we apply the the Cauchy-Schwarz inequality in the L^2 inner product: for all $f \in \mathcal{H}$,

$$\langle f^3 \rangle^2 \leq \langle f^2 \rangle \langle f^4 \rangle.$$

Applying this in (3.6) gives

$$
\begin{aligned}
\delta_m \mathcal{F}[f] \quad &\geq \quad b(f,f) - m^2 \frac{\langle f^3 \rangle^2}{\langle f^4 \rangle} \\
&\geq \quad b(f,f) - m^2 \langle f^2 \rangle.
\end{aligned}
\tag{3.10}
$$

Hence if

$$\inf \left\{ b(f,f) - m^2 \langle f^2 \rangle \ \middle| \ f \in \mathcal{H}, f \neq 0 \right\} \geq 0$$

or equivalently,

$$\inf \left\{ b(f,f) - m^2 \langle f^2 \rangle \ \middle| \ \|f\|_{\mathcal{H}} = 1 \right\} \geq 0,$$

$u \equiv m$ is a global minimizer of $\mathcal{F}$ over $\mathcal{H}_m$. If the inequality is strict, v is the unique global minimizer.

By invoking the correspondence of the Rayleigh quotient and the eigenvalues of the associated operator, we can equivalently rephrase in terms of eigenvalues involving B, the self-adjoint operator on $\mathcal{H}$ associated with $b(f,f)$, of the eigenvalue problem

$$(B - 2m^2)\psi \quad = \quad \lambda \psi. \tag{3.11}$$

Then if the smallest eigenvalue λ_1 is positive then $u \equiv m$ is a global minimizer of $\mathcal{F}$ over $\mathcal{H}_m$. Given b (i.e. B), we can readily compute this smallest eigenvalue which will depend on the exact size of the torus Ω. On the other hand, one can easily compute a lower bound, exact in the limit where the torus size tends to ∞, by transforming to Fourier space (Fourier series) and optimizing in the Fourier variable $|\mathbf{k}|$, treated as a continuous variable. To this end, for the Ohta-Kawaski functional, the operator

$$B - 2m^2 \quad = \quad \frac{1}{\gamma^2}(-\triangle) + (-\triangle)^{-1} + (m^2 - 1),$$

<hr>

[5]For (**OK**)

$$B = \gamma^{-2}(-\Delta) + (-\Delta)^{-1} + (3m^2 - 1),$$

while for (**PFC**),

$$B = (1 + \Delta)^2 + (3m^2 - \epsilon).$$

12

in Fourier space (defined on the flat torus with size $L \times L$) is multiplication by

$$\frac{1}{\gamma^2}|\mathbf{k}_{12}|^2 + |\mathbf{k}_{12}|^{-2} + (m^2 - 1)$$

where $|\mathbf{k}_{12}| = 2\pi L^{-1}(n_1, n_2)$ for integers (n_1, n_2), with $n_1^2 + n_2^2 \neq 0$. Optimizing $|\mathbf{k}_{12}|$, treated as a continuous variable, implies that this factor is always positive if

$$
\begin{aligned}
\lambda_1 &= \min_{\mathbf{k}_{12}} \frac{1}{\gamma^2}|\mathbf{k}_{12}|^2 + |\mathbf{k}_{12}|^{-2} + (m^2 - 1) \\
&\geq \min_{k \in \mathbb{R}} \frac{1}{\gamma^2}k^2 + k^{-2} + (m^2 - 1) \\
&= \frac{2}{\gamma} + (m^2 - 1) \geq 0.
\end{aligned}
$$

In the limit as the torus size $L \to \infty$, there are values of $\mathbf{k}_{12}$ arbitrarily close to the optimal (continuous) k. The excess energy for **(OK)** about the disordered state then satisfies

$$
\begin{aligned}
\delta_m \mathcal{F}[f] &\geq b_1(f, f) - m^2 \langle f^2 \rangle \\
&= \int_\Omega \frac{1}{2}\gamma^{-2}|\nabla f|^2 + \frac{1}{2}|\nabla(-\Delta)^{-1}f|^2 + \frac{1}{2}(m^2 - 1)f^2 \, d\mathbf{x} \\
&\geq \int_\Omega \frac{1}{\gamma}f^2 + \frac{1}{2}(m^2 - 1)f^2 \, d\mathbf{x} \\
&= \left(\frac{1}{\gamma} + \frac{1}{2}(m^2 - 1)\right) \int_\Omega f^2 \, d\mathbf{x}.
\end{aligned}
\tag{3.12}
$$

We conclude that if

$$\gamma \leq \frac{2}{1 - m^2} \tag{3.13}$$

then $\delta_m \mathcal{F}[f] \geq 0$ for all $f \in \mathcal{H}$, i.e., $u \equiv m$ is a global minimizer of **(OK)** over $u \in \mathcal{H}_m$. This proves a lower bound on the ODT which, except at $m = 0$, is far from optimal: This was essentially the approach taken in [6] (see also [14]).

For the Phase-Field Crystal functional, the analogous steps give that if

$$\epsilon \leq m^2 \tag{3.14}$$

then $u \equiv m$ (the liquid phase) is a global minimizer of **(PFC)** over $u \in \mathcal{H}_m$.

3.2 An improved quadratic lower bound.

In this subsection we derive an improved quadratic lower bound by exploiting the structure of B. Generally speaking, we aim to tighten the two consecutive inequality approximations ((3.4) and Cauchy-Schwarz) used in the previous subsection. Here the gap in the lower bound comes from the drastically different nature in the functions which i) optimize Cauchy-Schwarz, and ii) optimize the quadratic term (3.10) involving $b(f, f)$. Ideally, we may improve the lower bound if we use a sequence of inequalities which have *almost* the same optimizing functions.

Our new approach therefore relies on first using the Cauchy-Schwarz inequality in the more natural $b(f, f)$ inner product, followed by a constrained optimization problem involving B.

We write

$$\langle f^3 \rangle = \left\langle f\left(f^2 - \overline{f^2}\right)\right\rangle = \left\langle f B B^{-1}\left(f^2 - \overline{f^2}\right)\right\rangle$$

to find that

$$\begin{aligned}
\langle f^3 \rangle^2 &= \left\langle f B B^{-1}\left(f^2 - \overline{f^2}\right)\right\rangle^2 \\
&= \left\langle f, B^{-1}\left(f^2 - \overline{f^2}\right)\right\rangle_b^2 \\
&\leq \langle f, f \rangle_b \left\langle B^{-1}\left(f^2 - \overline{f^2}\right), B^{-1}\left(f^2 - \overline{f^2}\right)\right\rangle_b & (3.15) \\
&= 2b(f, f)\left\langle \left(f^2 - \overline{f^2}\right), B^{-1}\left(f^2 - \overline{f^2}\right)\right\rangle & (3.16)
\end{aligned}$$

In line (3.15) we used the Cauchy-Schwarz inequality in the inner product $\langle f, g \rangle_b$. The operator B^{-1} is defined on $\mathcal{H}$. We can extend B^{-1} to all of H^k by defining B^{-1} to be zero on constants. In other words, its extension to H^k is simply composition of B^{-1} with projection $\mathcal{P}$ onto $\mathcal{H}$. Abusing notation slightly, let us use B^{-1} to also denote the extension. Thus, by (3.16)

$$\langle f^3 \rangle^2 \leq 2b(f, f)\left\langle \left(f^2 - \overline{f^2}\right), B^{-1}\left(f^2 - \overline{f^2}\right)\right\rangle = 2b(f, f)\left\langle f^2, B^{-1}f^2\right\rangle \qquad (3.17)$$

Thus (3.17) implies

$$\frac{\langle f^3 \rangle^2}{b(f, f)\langle f^4 \rangle} \leq 2\frac{\left\langle f^2, B^{-1}f^2\right\rangle}{\langle f^4 \rangle}.$$

Since

$$\max_{f \in \mathcal{H}, f \neq 0} \frac{\left\langle f^2, B^{-1}f^2\right\rangle}{\langle f^4 \rangle} \leq \max_{g \geq 0, g \neq 0} \frac{\left\langle g, B^{-1}g\right\rangle}{\langle g^2 \rangle}, \qquad (3.18)$$

we define

$$r := \max_{g \geq 0, g \neq 0} \frac{\left\langle g, B^{-1}g\right\rangle}{\langle g^2 \rangle}. \qquad (3.19)$$

Note that for all functionals, B^{-1}, extended to H^k, is a bounded linear self-adjoint operator, and (3.19) is a constrained Rayleigh quotient. Combining (3.6), (3.17) and (3.19), we have the following prescription for the quadratic functional $Q[f]$

$$\delta_m \mathcal{F}[f] \geq Q[f] \quad \text{where} \quad Q[f] := (1 - 2m^2 r)b(f, f).$$

Lastly note that if $1 - 2m^2 r \geq 0$, the disordered state $u(\mathbf{x}) \equiv m$ is a global minimizer of $\mathcal{F}$. We summarize the previous calculations in the following theorem:

Theorem 3.1. *Let* $-1 < m < 1$ *and consider any functional* $\mathcal{F}$ *of the form* (2.2) *defined over*

$$\mathcal{H}_m = \left\{ u \,\middle|\, u = m + f, f \in \mathcal{H} \right\}.$$

Define the bilinear form b *on* $\mathcal{H}$ *by* (3.2) *and assume, without loss of generality, that* (3.3) *holds true. Let* B *be the associated operator on* $\mathcal{H}$ *defined by* (3.8)-(3.9) *extended, by projection, to all of* H^k. *Finally let* r *be given by* (3.19). *Then*

$$if \quad 1 - 2m^2 r \geq 0, \qquad u(\mathbf{x}) \equiv m \text{ is a global minimizer of } \mathcal{F}.$$

3.3 Solving for r.

To solve for r one must maximize a Rayleigh quotient (3.19), restricted to a convex set of functions

$$K_1 = \{g \,|\, g(\mathbf{x}) \geq 0\}$$

For numerical purposes, we can further rephrase the problem (3.19) as a maximization of a quadratic (convex) functional over a convex set of functions. First, we may remove the denominator in (3.19) as follows. Introduce the ball of functions

$$K_2 = \{g \,|\, \langle g^2 \rangle \leq 1\}.$$

We note that K_2 is convex, and hence $K = K_1 \bigcap K_2$ is also convex. The problem (3.19) may then be rephrased as

$$r = \max_{g(\mathbf{x}) \in K} \langle gB^{-1}g \rangle. \tag{3.20}$$

For a constrained convex optimization problem, the Karush-Kuhn-Tucker (KKT) conditions describe the criteria for an optimal $g(\mathbf{x})$ in (3.20). Namely, optimality occurs when the gradient of the functional $(2B^{-1}g)$ in (3.20) lies within the normal cone $\mathcal{N}_g(K)$ of the feasible set

$$2B^{-1}g \in \mathcal{N}_g(K) \quad \text{where} \quad \mathcal{N}_g(K) = \left\{ u \,\middle|\, \langle h - g, u \rangle \leq 0, \,\forall\, h \in K \right\}. \tag{3.21}$$

To describe the normal cone at a location g, we introduce the positive variables $y(\mathbf{x}) \geq 0$ and $\lambda \geq 0$. When $g(x)$ is on the boundary of the feasible set, for instance $g(x_0) = 0$ for some x_0, then the normal cone contains functions which are negative at $x = x_0$. Here we use $y(\mathbf{x})$ and λ to parameterize such functions. To do so, first introduce a sum over all constraints

$$\mathcal{L} = -2 \int_\Omega y(\mathbf{x})g(\mathbf{x}) \, \mathrm{d}\mathbf{x} + \lambda \left(\langle g^2 \rangle - 1 \right).$$

The normal cone is then given by the (L^2) variational derivative $\frac{\delta\mathcal{L}}{\delta g}$

$$\mathcal{N}_g(K) \;=\; \left\{ \frac{\delta\mathcal{L}}{\delta g} \;\middle|\; y(\mathbf{x}) \geq 0,\; \lambda \geq 0,\; y(\mathbf{x})g(\mathbf{x}) = 0,\; \lambda\left(\langle g^2\rangle - 1\right) = 0 \right\}.$$

Equating the gradient of the functional (3.20) with the normal cone parameterization, we arrive at the KKT conditions for optimality

$$B^{-1}g \;=\; -y + \lambda g \tag{3.22}$$

with

$$g(\mathbf{x})y(\mathbf{x}) \;=\; 0, \quad g(\mathbf{x}) \;\geq\; 0, \quad y(\mathbf{x}) \;\geq\; 0, \quad (\langle g^2\rangle - 1)\lambda \;=\; 0. \tag{3.23}$$

Here $y(\mathbf{x})$ and λ are the Lagrange multipliers for the constraints. Using the conditions (3.23), we can partially solve (3.22) as

$$y \;=\; (-B^{-1}g)_+ \quad \text{and} \quad \lambda g \;=\; (B^{-1}g)_+ \tag{3.24}$$

Here $f(x)_+ = \frac{1}{2}(f + |f|)$ is the non-negative component of a function. Physically, $(B^{-1}g)_+$ represents the component of the gradient $B^{-1}g$ inside the set K_1.

Remark 1. The value r from (3.19) corresponds to the largest λ satisfying the KKT condition (3.22).

Since we cannot solve (3.24) exactly, we numerically maximize (3.20) and use (3.24) as a stopping criterion. We do so by performing a modified power iteration. Here we work on a regular grid with N grid points $x_k = kh$ for $0 \leq k \leq N - 1$, and grid spacing $h = L/N$ where $L = L_x = L_y$ is the size of the domain. Letting $g_{ij} = g(x_i, y_j)$ denote the discrete values of g on the grid we estimate r via the following algorithm. When g^n is deep inside the feasible set, $(B^{-1}g^n)_+$ is always non-negative, and the algorithm reduces to a standard power iteration. When g^n is on the boundary of the feasible set K, the algorithm is a power iteration restricted to the tangent of the feasible set. Figure 4 outlines the evolution of δ and r versus the number of iterations for (**OK**), while figure 5 shows a plot of the solutions $g(\mathbf{x})$ and $y(\mathbf{x})$. For the functionals and parameter values we consider, the modified power iteration algorithm achieves machine precision for δ within 10^5 iterations.

Remark 2. The algorithm converges to a KKT point which is a necessary condition for optimality. At this point we do not have a proof that for the functionals under consideration, satisfying a stable KKT condition is also sufficient for global optimality. More specifically, maximizing a convex function over a convex set via gradient flow may have multiple stable KKT points. In our case, we have repeated the numerics with random initial data and have only observed convergence to a unique maximizer.

(Modified power iteration)

1. Initialize g^0:

$$g_{ij}^0 = \beta \sigma_{ij}$$

   where β is an appropriate normalization constant. The σ_{ij} are independent random samples (i.i.d.) from a uniform distribution $0 \leq \sigma_{ij} \leq 1$.

2. Iterate via

$$\begin{aligned} g^{n+1} &= \beta^n (B^{-1} g^n)_+ \\ &= \beta^n (\mathcal{F}^{-1} B^{-1} \mathcal{F} g^n)_+ \end{aligned}$$

   Here β^n is just a rescaling to ensure $\langle (g^{n+1})^2 \rangle = 1$. To efficiently compute the operator $(B^{-1} g^n)$ we use a fast Fourier transform (FFT) $\hat{g}(\mathbf{k}) = \mathcal{F} g$ and exploit the fact that B^{-1} is a diagonal operator in Fourier space.

3. Stopping criteria: let

$$\begin{aligned} \lambda &= \int_\Omega g(B^{-1}g)_+ \, d\mathbf{x} \\ \delta &= \frac{1}{|\Omega|^{1/2}} ||(B^{-1}g)_+ - \lambda g||. \end{aligned}$$

   Here δ is the volume averaged L^2 norm of the error in the KKT condition. Iterate until a δ achieves a pre-described tolerance. In our case we typically control $\delta \leq 10^{-8}$. The exact solution to (3.24) has $\delta = 0$.

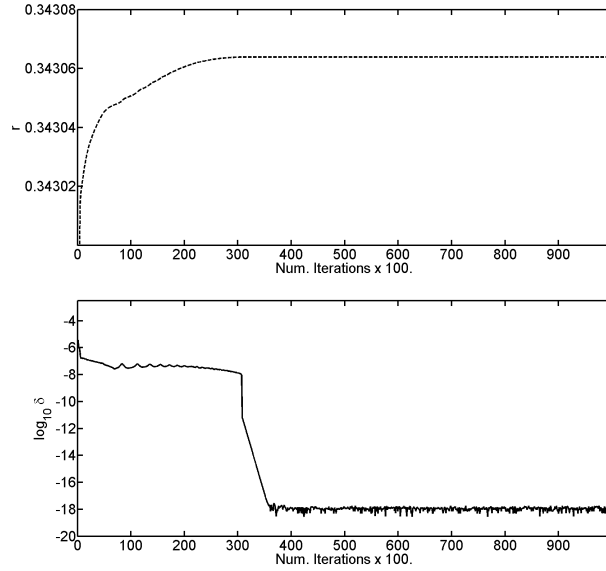Figure 4: Top: Plot of the value r (dashed line) versus the number of iterations in the modified power iteration algorithm. Bottom: norm δ (solid line) versus number of iterations. Here $m = 0.9$ and $\gamma = 2.1$. The norm δ achieves machine precision by $\sim 4 \times 10^4$ iterations.
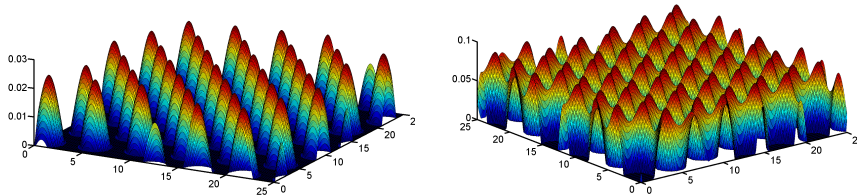

Figure 5: (**OK**) with $m = 0.25$, $\gamma = 2.35$. Left: plot of the maximizer $g(\mathbf{x})$ to (3.19). Right: plot of the Lagrange multiplier function $y(\mathbf{x})$ which arises in solving the optimization problem (3.19). Note that $y(\mathbf{x}) \geq 0$ and $g(\mathbf{x}) \geq 0$ have disjoint supports.
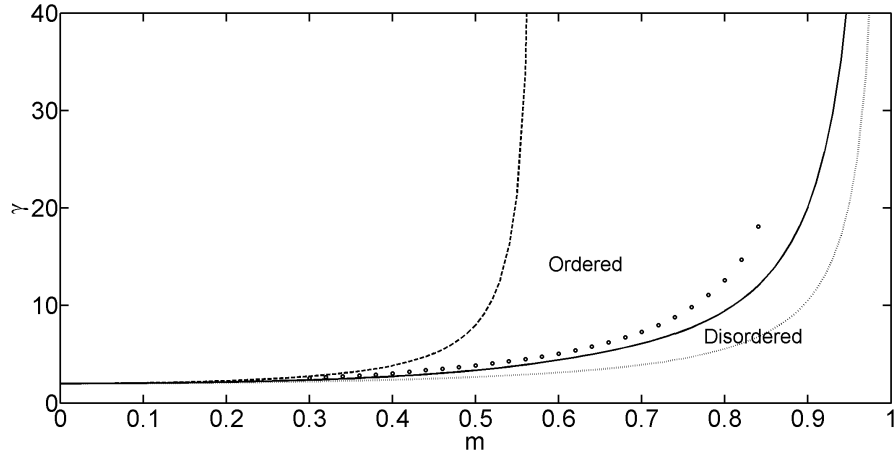
Figure 6: Plot of the ODT curve for (**OK**). The solid line is the lower bound estimate using (3.19), the dashed line is the conventional linear stability curve, while the circles (O) are a numerical approximation to the exact ODT curve (they represent the smallest γ with a function $u(\mathbf{x})$ having lower energy than $u = m$). Here the upper and lower bound computations are performed on a domain $8\pi \times 8\pi$ and $N = 256$ grid points. The bottom dotted curve is the less optimal lower bound estimate (3.13).
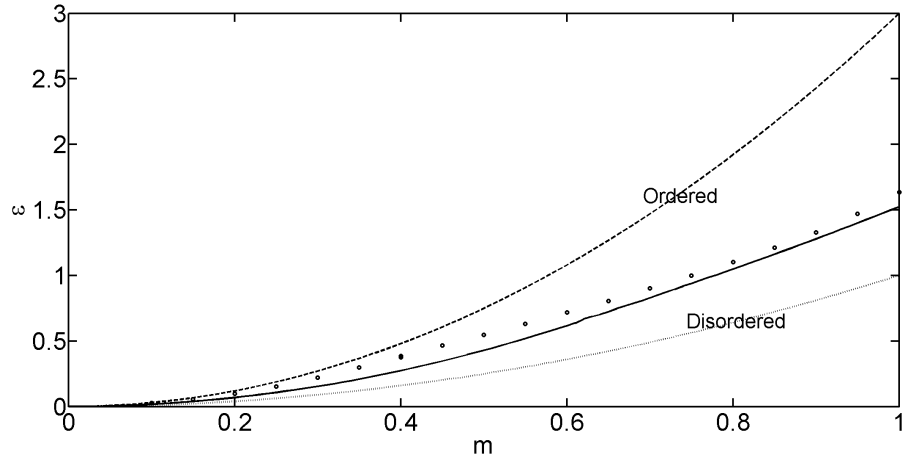

Figure 7: Plot of the ODT curve for (**PFC**). The solid line is the lower bound estimate using (3.19), the dashed line is the conventional linear stability curve, while the circles (O) are a numerical approximation to the exact ODT curve. The bottom dotted curve is the less optimal lower bound estimate (3.14).
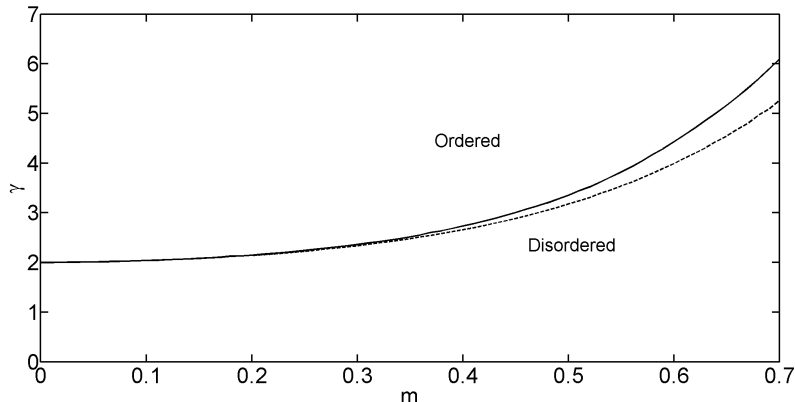
19

Figure 8: Computed lower bound of the ODT curve for (**OK**) in $3D$ (bottom dashed) vs. the $2D$ bound (top solid) of Figure 6.

3.4 Results for the ODT and their optimality.

In the following section we numerically compute an upper and lower bound to the ODT curve for the two functionals (**OK**) and (**PFC**). Specifically, for the lower bound we seek to characterize the curve in the phase diagram (m, γ_c) or (m, ϵ_c) where $1 - 2m^2 r = 0$. Such a curve partitions the phase diagram so that in one region m is the global minimum, i.e., the region where $1 - 2m^2 r \geq 0$. In our case, we solve for r using the modified power iteration algorithm outlined in the previous section with 2×10^4 iterations to ensure that the stopping criteria of $\delta \leq 10^{-8}$ is reached. We also note that r can depend on m, γ or ϵ depending on the functional at hand. To compute the curve, we fix a value of m and perform a root finding algorithm to solve for γ_c (or ϵ_c) such that $1 - 2m^2 r = 0$. Specifically, we use a bisection algorithm and solve for the critical γ_c with a tolerance of $|1 - 2m^2 r| \leq 10^{-5}$. It is important to note that for a fixed value of m, the ratio r is monotonic in the parameters γ (or ϵ)[6]. Hence, the root finding algorithm converges to the single root, and the curve γ_c versus m partitions the phase plane into distinct regions.

The solid curves in Figures 6 and 7 show the numerical lower bound for the ODT curve.

In addition to the numerical computation of a lower bound on the ODT curve, we also obtain an upper bound by *searching* for states which have an energy lower than the constant $u = m$. We emphasize again that since the functionals are non-convex, we have no guarantee

---

[6]Observe that for two values $\gamma_1 < \gamma_2$, the difference in the associated operators $B_2 - B_1$ is positive definite. Indeed, $B_1 - B_2 = -\left(\gamma_1^{-2} - \gamma_2^{-2}\right)\Delta$, and multiplying each side first on the left by B_1^{-1} and then on the right by B_2^{-1}, we have

$$B_2^{-1} - B_1^{-1} = \left(\gamma_1^{-2} - \gamma_2^{-2}\right)B_1^{-1}\left(-\Delta\right)B_2^{-1}$$

But $B = B_1^{-1}(-\Delta)B_2^{-1}$ is the product of three self-adjoint, positive definite operators, and on the torus, B_1, $(-\Delta)$, B_2 all mutually commute. As a result B is self-adjoint and positive definite (one can use the complete set of common eigenfunctions to show that every eigenvalue of B is positive). It follows that for any function $g(\mathbf{x}) \neq 0$, we have $\langle g, B_2^{-1}g \rangle > \langle g, B_1^{-1}g \rangle$. This proves that the associated ratios r_2 and r_1 corresponding to γ_2 and γ_1 satisfy $r_2 > r_1$. An identical argument holds for ϵ in (**PFC**).
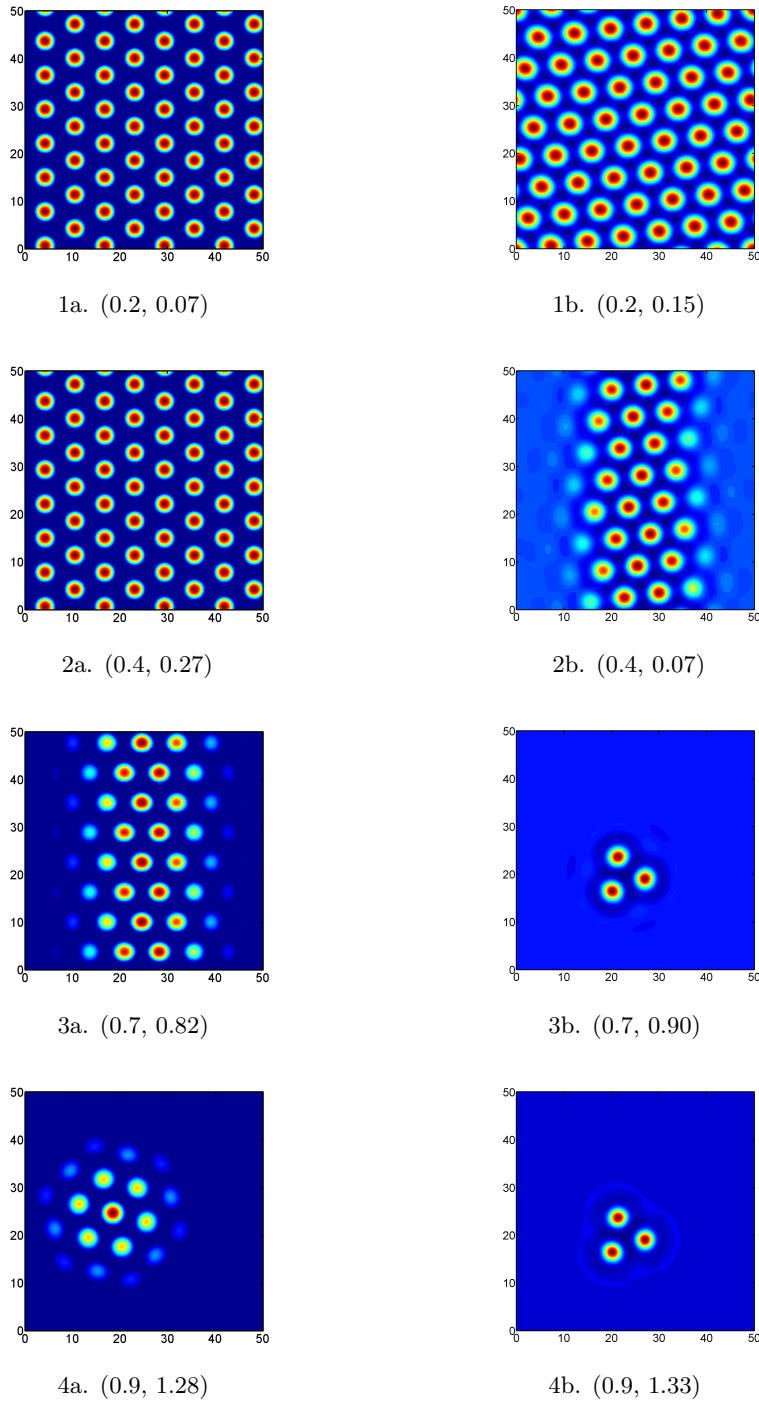
1a. (0.2, 0.07)

1b. (0.2, 0.15)

2a. (0.4, 0.27)

2b. (0.4, 0.07)

3a. (0.7, 0.82)

3b. (0.7, 0.90)

4a. (0.9, 1.28)

4b. (0.9, 1.33)

Figure 9: Computations for (**PFC**). Left column 1a-4a: Plot of the maximizer $g(\mathbf{x})$ to (3.19) for (**PFC**). Values are reported as (m, ϵ). Right column 1b-4b: Plot of the computed metastable pattern associated with the smallest ϵ for which one could simulate a pattern having lower energy than $u = m$. Images beside each other occur at the same value of m, but with different ϵ - the left and right being lower and upper bounds on the ODT respectively. Note that there are strong similarities in the patterns of $g(\mathbf{x})$ and the approximate critical (large) perturbations from the constant state.

21

that the upper bound is close to optimal. To obtain an upper bound curve, we first fix a value of m. We then vary the parameter γ (or ϵ) looking for the smallest value at which there exists a state $u \neq m$ with $\mathcal{F}[u] \leq \mathcal{F}[m]$. The circles in Figure 6 correspond to the smallest value of γ we found with such a state. As a result, the true ODT curve in Figure 6 lies below the circles and above the solid curve. To determine if a specific value of m and γ (or ϵ) has a non-constant minimizer $u \neq m$, we start with a candidate initial data $u(\mathbf{x}, 0) = u_0(\mathbf{x})$ and run a gradient flow for some time $T \leq 50$ to minimize the energy. We then check if the energy $\mathcal{F}[u(\mathbf{x}, T)] \leq \mathcal{F}[m]$. We then repeat the process to find the best upper bound γ_{UB} yielding states with energy lower than the constant state $u = m$. In this approach, the error in γ_{UB} with the true ODT curve depends on how close $u(\mathbf{x}, T)$ is to the global minimizer. As a result, the quality of the upper bound depends on how well one chooses $u_0(\mathbf{x})$. In our case, we try several initial conditions $u_0(\mathbf{x})$ and take the smallest γ found over all trials as our upper bound γ_{UB}. Specifically, for the functional (**OK**) we try initial data $u_0(\mathbf{x})$ i) corresponding to a pure hexagonal lattice, ii) a single point mass, iii) a non-perfect hexagonal array with defects.

We also performed a 3D computation based upon (3.19) for the ODT of (**OK**). In Figure 8 we plot the 3D computed ODT (a lower bound) and the 2D one presented in Figure 6. As expected, the 3D curve lies below the 2D. Note that for 3D we only computed the curve up to $m = 0.7$. Computation for larger m can readily be performed but requires more CPU time. All our computations were done in MATLAB.

Finally, we observe that in some cases the computed function $g(\mathbf{x})$ accurately predicts the pattern of minimizers. For instance Figure 9 shows a comparison of optimal functions associated with both the numerically estimated upper bound (optimal u) and the computed lower bound (optimal g). Close to the ODT and $m = 0$, the optimal $g(\mathbf{x})$ accurately predicts the pattern of what is believed to be the global minimizer, including the correct lattice size.

Remark 3. The computed lower bound (3.19) and the numerical upper bound in Figures 6 and 7 have a small gap. The gap is due to the fact that i) the upper bound is only a numerical investigation and is not sharp (in fact the numerics become increasingly difficult with large values of m), and ii) our lower bound is not sharp. In the case of our lower bound, we use the estimate (3.17) which is sharp for functions of the form

$$\alpha f = B^{-1} f^2 \tag{3.25}$$

for some α. Meanwhile, optimizers of the ratio (3.19) satisfy the KKT condition (3.22). If every function of the form (3.25) also satisfied the KKT condition, then our lower bound would be exact. The gap is therefore partially due to the fact the functions do not simultaneously satisfy (3.25) and (3.22).

4   Analysis for Non-Constant Metastable States

We now discuss how to extend our method to non-constant states. Here we adopt the approach taken from section 3, but apply the inequalities to non-constant candidate minimizers v. Since the initial steps are elementary and short but essential, we repeat them here. We consider stable critical points (states with vanishing first and non-negative second variations) and derive sufficiency conditions for global minimality based upon our two approaches for quadratic lower

bounds. Unfortunately except for the constant state, we have no exact representative of critical points for any of the functionals considered here. Hence our methods must be directly coupled with numerics whereby we

- compute a metastable state (candidate minimizer) v for which the appropriate energy gradient is small,
- address the sufficiency conditions for global minimality.

In our approaches, the lower bound takes the following form

$$\mathcal{F}[v + f] - \mathcal{F}[v] \geq C\langle f^2 \rangle, \tag{4.1}$$

where the constant C, dependent on the material parameters, is obtained numerically.

Let $-1 < m < 1$ and suppose v is a candidate for a global minimizer over $u \in \mathcal{H}_m$. In particular, we may assume that v

- Is a critical point in the sense that for all $f \in \mathcal{H}$ the first variation in direction f vanishes, i.e.,

$$\forall\, f \in \mathcal{H} \qquad 2a(v, f) - \int_\Omega v(1 - v^2)f \; \mathrm{d}\mathbf{x} = 0. \tag{4.2}$$

- The second variation is positive semi-definite $\forall\, f \in \mathcal{H}$, $b(f, f) \geq 0$, i.e.,

$$b(f, f) = a(f, f) + \int_\Omega \left(\frac{3v^2}{2} - \frac{1}{2} \right) f^2 \; \mathrm{d}\mathbf{x} \geq 0. \tag{4.3}$$

In all subsequent numerical calculations, we always numerically verify that $b(f, f)$ is positive semi-definite for any candidate minimizer v.

As in (3.1), we compute the excess energy $\delta_v \mathcal{F}$ about a state v satisfying (4.2): for all $f \in \mathcal{H}$

$$
\begin{aligned}
\delta_v \mathcal{F}[f] &= \mathcal{F}[v + f] - \mathcal{F}[v] \\
&= a(f, f) + \int_\Omega \left(\frac{3v^2}{2} - \frac{1}{2} \right) f^2 + vf^3 + \frac{f^4}{4} \; \mathrm{d}\mathbf{x} \\
&= b(f, f) + \int_\Omega vf^3 + \frac{f^4}{4} \; \mathrm{d}\mathbf{x},
\end{aligned}
\tag{4.4}
$$

where

$$b(f, g) = a(f, g) + \int_\Omega \left(\frac{3v^2}{2} - \frac{1}{2} \right) f\, g \; \mathrm{d}\mathbf{x}.$$

Note that the linear terms in f (which are precisely the left hand side of (4.2)) vanish since v is a critical point.

As with the previous case where $v \equiv m$, if b is positive-definite, we will make use of the inner product on $\mathcal{H}$ induced by b:

$$\langle f, g \rangle_b := 2b(f, g). \tag{4.5}$$

and the self-adjoint operator B defined on $\mathcal{H}$ by

$$\langle f, g \rangle_b =: \langle f, Bg \rangle \qquad \text{or} \qquad b(f,g) = \frac{1}{2} \langle f, Bg \rangle \tag{4.6}$$

By composing both B and its inverse B^{-1} with the projection operator defined on $\mathcal{H}_m$

$$\mathcal{P}u = u - \fint u \, d\mathbf{x},$$

we may extend both B and B^{-1} to all of H^k. While we do not rename these extensions, note that on $\mathcal{H}_m$

$$B \circ B^{-1} = \mathcal{P}.$$

In Sections 4.1 and 4.2, we first give the details for two lower bounds via inequalities analogous to the respective ones of Sections 3.1 and 3.2. However, in each case we note that the resulting sufficiency conditions are *empty* as a result of the inherent symmetry invariance of the energy on the torus. By restricting to the Ohta-Kawasaki function, we then present a preliminary analysis of these symmetry issues by

1. addressing the global optimality of the lamellar phase in 1D and 2D space (Sections 4.3 and 4.4);

2. addressing the global optimality of the lamellar phase when the domain is a rectangular torus (Section 4.5);

3. addressing global optimality of a metastable state for a perturbed (OK) functional which includes a spatially non-symmetric potential (Section 4.6).

4.1 First quadratic lower bound.

As in Section 3.1, the first lower bound comes from elementary inequalities. There we used an elementary pointwise inequality (3.4) combined with the L^2 Cauchy-Schwarz inequality. Note that we can combine these two into one elementary pointwise inequality: For any real numbers α and β, $\beta^2 (\beta/2 + \alpha)^2 \geq 0$ implies that

$$\alpha \beta^3 + \frac{\beta^4}{4} \geq -\alpha^2 \beta^2. \tag{4.7}$$

Applying this pointwise to $\alpha = v$ and $\beta = f$, we find from (4.4) that

$$\delta_v \mathcal{F}[f] \geq b(f,f) - \int_\Omega v^2 f^2 \, d\mathbf{x}. \tag{4.8}$$

Now let $-1 < m < 1$ and consider any functional $\mathcal{F}$ of the form (2.2) defined over $\mathcal{H}_m$. Let $v \in \mathcal{H}_m$ be a critical point of $\mathcal{F}$ in the sense that (4.2) holds true. Then (4.4) implies that if

$$\inf \left\{ b(f,f) - \langle v^2 f^2 \rangle \;\middle|\; f \in \mathcal{H}, f \neq 0 \right\} \geq 0$$

$$\left(\text{or equivalently} \quad \inf\left\{ b(f,f) - \langle v^2 f^2 \rangle \;\middle|\; \|f\|_{\mathcal{H}} = 1 \right\} \geq 0\right),$$

v is a global minimizer of $\mathcal{F}$ over $\mathcal{H}_m$. If the inequality is strict, v is the unique global minimizer. Alternatively, if λ_1 is the first eigenvalue of the corresponding eigenvalue problem

$$(B - 2v^2)\psi \;=\; \lambda\psi, \tag{4.9}$$

then we let

$$C_1 := \lambda_1.$$

If $C_1 \geq 0$, then v is a global minimizer of $\mathcal{F}$ over $\mathcal{H}_m$. If the inequality is strict, v is the unique global minimizer.

This is our first sufficiency condition. However, we immediately note that, except for $v \equiv m$, the condition $C_1 \geq 0$ may never hold true, suggesting that, except for the constant phase, this strategy requires additional ideas. In fact, it is straightforward to see that this is the case for periodic boundary conditions! For instance, small translations in the x direction $f(\mathbf{x}) = v(x + s, y) - v(\mathbf{x}) \approx s\frac{\partial v}{\partial x}$ will leave the energy unchanged. To show that such directions imply $C_1 < 0$, first note that $v(\mathbf{x})$ solves the Euler-Lagrange equation (4.2), and hence v itself is always an eigenvalue of $B - 2v^2$ with corresponding eigenvalue 0, that is,

$$(B - 2v^2)v \;=\; 0. \tag{4.10}$$

Moreover, in our case of periodic boundary conditions, a minimizer can always be translated with no cost to the energy, and this implies that one always has $\lambda_1 < 0$. To see this let $v_x = \partial_x v$ be a derivative of $v(\mathbf{x})$ (which can be in any direction). Recall that our operator B associated with the bilinear form

$$b(f,g) \;=\; a(f,g) + \int_\Omega \left(\frac{3v^2}{2} - \frac{1}{2} \right) f\,g \; \mathrm{d}\mathbf{x},$$

is defined by (3.8) and (3.9). Translational symmetry of the energy functional implies that the part of the operator, say A, associated with the form via $a(f,g) = \frac{1}{2}\langle f, Ag \rangle$ satisfies

$$(Au)_x \;=\; Au_x.$$

This is certainly the case for (**OK**) and (**PFC**) on the torus. Hence using $B = A + 3v^2 - 1$ and differentiating (4.10) we find

$$\begin{aligned}
0 &= (Bv - 2v^3)_x \\
&= (Av + v^3 - v)_x \\
&= (Av_x + 3v^2 v_x - v_x) \\
&= Bv_x.
\end{aligned}$$

If we normalize $\tilde{v}_x = cv_x$ so that $\|\tilde{v}_x\| = 1$, we obtain the following bound

$$\langle \tilde{v}_x, (B - 2v^2)\tilde{v}_x \rangle = -2\|v\,\tilde{v}_x\|^2 < 0.$$

4.2 Second quadratic lower bound.

In the second approach (analogous to that of Section 3.2), we exploit the structure of b, the (local) second variation, by invoking the Cauchy-Schwarz inequality with respect to the associated B-norm. To this end, using the trivial inequality (3.4) we have

$$\begin{aligned}
\mathcal{F}[v+f] - \mathcal{F}[v] &= b(f,f) + \langle vf^3 \rangle + \frac{1}{4}\langle f^4 \rangle \\
&\geq b(f,f) - \frac{\langle vf^3 \rangle^2}{\langle f^4 \rangle}
\end{aligned}$$

Thus we obtain the following lower bound

$$\mathcal{F}[v+f] - \mathcal{F}[v] \geq (1-2r)b(f,f),$$

where

$$r := \frac{1}{2} \sup_{f \in \mathcal{H}_m} \frac{\langle vf^3 \rangle^2}{b(f,f)\langle f^4 \rangle}.$$

Next let us further assume that b is positive-definite, i.e.,

$$b(f,f) > 0, \quad \forall f \neq 0.$$

Unlike for the constant state, this assumption is not harmless. Indeed it will never hold true on the torus for all $f \in \mathcal{H}$, and we will have to restrict our perturbation Hilbert space by projecting out certain directions related to symmetries. For the time being, let us assume that $b(f,f) > 0$ for all $f \neq 0$ in perhaps some subspace of $\mathcal{H}$.

To obtain the new lower bound coefficient we follow the same procedure as in Section 3.2, and bound r using the Cauchy-Schwarz inequality with respect to the b induced inner product (defined in (4.5) and (4.6)). We find

$$\begin{aligned}
r &= \frac{1}{2} \sup_{f \in \mathcal{H}} \frac{\langle B^{-1}vf^2, Bf \rangle^2}{b(f,f)\langle f^4 \rangle} \\
&\leq \sup_{f \in \mathcal{H}} \frac{\langle (vf^2), B^{-1}(vf^2) \rangle b(f,f)}{b(f,f)\langle f^4 \rangle} \\
&= \sup_{g(\mathbf{x}) \geq 0} \frac{\langle (vg), B^{-1}(vg) \rangle}{\langle g^2 \rangle} = r_0
\end{aligned} \tag{4.11}$$

Note now that again we have set $g = f^2$. We may then numerically optimize r_0 defined by (4.11) using the same algorithm as in the case where $v = m$ with one modification. Here we replace B^{-1} from algorithm 1 with $vB^{-1}v$, i.e., multiplication by v followed by B^{-1} and then again multiplication by v:

$$g^{n+1} = \beta^n \big((vB^{-1}v)g^n \big)_+$$

Here β^n is the appropriate normalization factor and $(\cdot)_+$ denotes the positive part of a function. We also take the initial data g^0 to be random.
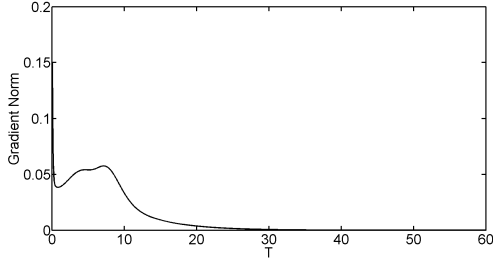
Figure 10: The L^2 norm of the gradient ($||v_t||$ from (4.12)) during the evolution of the gradient flow. The final state is the candidate lamellae v^l.

Finally we compute[7] the coefficient for the lower bound C_2 as

$$C_2 = (1 - 2r_0) \left(\min_{||f||=1} b(f,f) \right) = (1 - 2r_0)\frac{\lambda_b}{2}$$

where λ_b is the smallest eigenvalue of the operator B.

4.3   Analysis of the lamellar phase of (OK) in one dimension.

In one space dimension, it can indeed be proven that the global minimizer to (**OK**) on a periodic domain must be periodic [18, 21, 25]. We call such a periodic structure lamellar. Thus far, we have shown that neither of the results from Sections 4.1 or 4.2 are directly applicable to non-constant states v on a torus geometry. In this subsection, we show that if we introduce additional constraints in the search directions f, then we may use the ideas from section 4.1 to analyze non-constant candidate minimizers to (**OK**) in a 1D periodic domain. Specifically, we argue that, for certain parameters (m, γ), a computed lamellae structure is close to optimal.

We take $m = 0$, $\gamma = 2.5$ and a periodic domain $L_x = 4\pi$ and obtain the candidate minimizer $v^l(x)$ by running the H^{-1} gradient flow on random initial data. That is, we solve

$$v_t = -\gamma^{-2}\Delta^2 v + \Delta(v^3 - v) - (v - m), \tag{4.12}$$

with random initial conditions $v(x_j) = \sigma_j$, where x_j is the jth grid point and σ_j is a random number in $[-1/2, 1/2]$. The initial data is also projected to have an average m. We run the gradient flow (integration time $T \sim 1000$) with progressively smaller time steps so that the candidate minimizer solves the Euler-Lagrange equations to a required tolerance $\epsilon = 6 \times 10^{-8}$ (Figure 10). As a result, we obtain a candidate minimizer v^l, shown in Figure 11.

We now make several observations regarding the symmetries in $\mathcal{F}[v]$. Note that for any function $v(\mathbf{x})$, the following have the same energy:

---

[7]As a numerical note, we compute B^{-1} as follows. We build the following operator

$$Lf = \gamma^{-2}(\Delta^2)f - \Delta\big[(3v^2(\mathbf{x}) - 1)f\big] + f$$

and note that $B = (-\Delta)^{-1}L$. Hence the inverse can be computed as

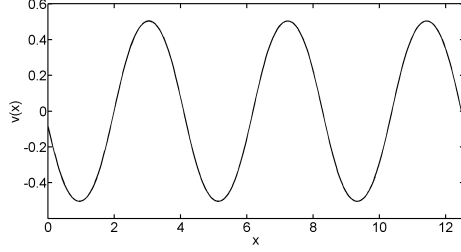$$g^{n+1} = \beta^n\big((vL^{-1}(-\Delta)v)g^n\big)_+$$

27

Figure 11: Candidate minimizer v^l for $m = 0$, $\gamma = 2.5$ on $1D$ periodic domain 4π.

- arbitrary translations: $v(x - s)$, for any constant s;
- inversion symmetry: $v(-x)$;
- flip about the vertical axis: $-v(x)$.

As a result of the collection of symmetries, the candidate minimizer v^l is not unique. We now constrain the search directions f to compute the lower bound coefficient C_1. Without loss of generality, one may restrict search directions f so that $f \in \mathcal{Z}$ where

$$\mathcal{Z} := \left\{ f \in \mathcal{H} \mid \langle f, e_1 \rangle = 0 \right\} \quad \text{where} \quad e_1 := \partial_x v^l. \tag{4.13}$$

To see this note that given any candidate minimizer v and any global minimizer w, one can always find a translation s (which leaves the energy unchanged), such that $f = w(x - s) - v \in \mathcal{Z}$ is orthogonal to e_1. This is simply a fact about functions on the torus. First note that $\langle v, v_x \rangle = 0$. Then, given two functions $v(x)$ and $w(x)$ on the torus, one may always shift $w(x - s)$ so that $\langle w, \partial_x v \rangle = 0$. Let

$$h(s) \quad := \quad \int_0^{4\pi} w(x - s) \partial_x v(x) \, \mathrm{d}x.$$

By applying the Cauchy-Schwarz inequality and a standard density argument for w, we see that $h(s)$ is a continuous function of s. We now observe that

$$
\begin{aligned}
\int_0^{4\pi} h(s) \, \mathrm{d}s \quad &= \quad -\int_0^{4\pi} \int_0^{4\pi} \partial_x w(x - s) v(x) \, \mathrm{d}x \, \mathrm{d}s \\
&= \quad -\int_0^{4\pi} \left(\int_0^{4\pi} \partial_x w(x - s) \, \mathrm{d}s \right) v(x) \, \mathrm{d}x \\
&= \quad \int_0^{4\pi} \left(\int_0^{4\pi} \partial_s w(x - s) \, \mathrm{d}s \right) v(x) \, \mathrm{d}x \\
&= \quad 0.
\end{aligned}
$$

Hence by the mean value theorem, $\exists s^*$ such that $h(s^*) = 0$.

Thus it suffices to minimize the quadratic lower bound over a smaller subspace of search directions:

$$\inf \left\{ b(f, f) - \langle v^2 f^2 \rangle \mid f \in \mathcal{Z}, f \neq 0 \right\} \geq 0.$$

28

Here the constraint $f \in \mathcal{Z}$ modifies the eigenvalue problem (4.9) slightly to

$$\left(B - 2(v^l)^2\right)\psi = \lambda\psi + \kappa(\partial_x v^l) \quad \text{with} \quad \langle \psi, \partial_x v^l \rangle = 0 \tag{4.14}$$

where κ is a new Lagrange multiplier introduced to handle the orthogonality condition. The lower bound coefficient is then $C_1 = \lambda_1$, where λ_1 is the smallest (constrained) eigenvalue of (4.14).

To solve for λ_1 in (4.14), we numerically build the operator $(B - 2(v^l)^2)$ and project out the orthogonality constraints. Additional details are given in appendix A. This calculation yields

$$C_1 = \lambda_1 = 1.6 \times 10^{-6}.$$

We note however that the discretization errors in the calculation for C_1 are of $O(10^{-6})$. Hence for numerical purposes C_1 is zero. This is also consistent with the fact, shown in equation (4.10), that for an analytic critical point, the system (4.14) contains a zero eigenvalue corresponding to $\psi = v^l$. But what exactly does this imply in regard to v^l being a global minimizer? In our calculation yielding

$$\delta_{v^l}\mathcal{F}_1[f] \geq C_1 \int_\Omega f^2 \, \mathrm{d}\mathbf{x},$$

we assumed that

$$2a_1(v^l, f) - \int_\Omega v^l(1 - (v^l)^2)f \, \mathrm{d}\mathbf{x} = 0.$$

The extent to which this is true is measured by the tolerance via the size of the energy gradient

$$\mathrm{grad}_{H^{-1}}\mathcal{F}_1(v^l) = \gamma^{-2}(-\Delta)^2 v^l + (v^l - m) + (-\Delta)((v^l)^3 - v^l).$$

We ran the gradient flow sufficiently long so that

$$\|\mathrm{grad}_{H^{-1}}\mathcal{F}_1(v^l)\|_{H^{-1}} < \epsilon.$$

Integration by parts gives for any $f \in \mathcal{H}$,

$$\left\langle \mathrm{grad}_{H^{-1}}\mathcal{F}_1(v^l), (-\Delta)^{-1}f \right\rangle = 2a_1(v^l, f) - \int_\Omega v^l(1 - (v^l)^2)f \, \mathrm{d}\mathbf{x}.$$

On the other hand by (2.1),

$$\left|\left\langle \mathrm{grad}_{H^{-1}}\mathcal{F}_1(v^l), (-\Delta)^{-1}f \right\rangle\right| \leq \left\|\mathrm{grad}_{H^{-1}}\mathcal{F}_1(v^l)\right\|_{H^{-1}} \left\|(-\Delta)^{-1}f\right\|_{H^1}$$

$$= \left\|\mathrm{grad}_{H^{-1}}\mathcal{F}_1(v^l)\right\|_{H^{-1}} \|f\|_{H^{-1}}.$$

Hence,

$$\left|2a_1(v^l, f) - \int_\Omega v^l(1 - (v^l)^2)f \, \mathrm{d}\mathbf{x}\right| \leq \epsilon\|f\|_{H^{-1}}.$$

Thus, up to numerical errors, we have shown the following: If $w(x)$ is the global minimizer then

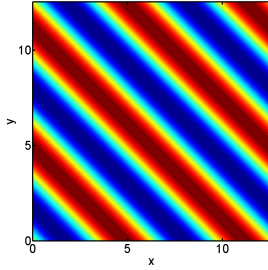$$\mathcal{F}_1[w] - \mathcal{F}_1[v^l] \geq -\epsilon\|f\|_{H^{-1}} + C_1\|f\|^2, \tag{4.15}$$

29

Figure 12: Candidate minimizer v^l for $m = 0$, $\gamma = 2.02$ with torus size to be $4\pi \times 4\pi$. Note that the orientation of the lamellae is exactly at $45°$.

where $f = w(x - s^*) - v^l$ for some s^*. Note that (4.15) puts the energy of v^l as being optimal up to the order of numerical errors. Indeed, we can crudely estimate $||f||_{H^{-1}}$ by noting that since $\mathcal{F}[w] \le \mathcal{F}[m] = |\Omega|\frac{(1-m^2)^2}{4}$, $||w||_{H^{-1}}^2 \le \pi$ and the same is true for v^l (here $m = 0$, $|\Omega| = 4\pi$). Hence $||f||_{H^{-1}} \le 2\sqrt{\pi}$. On the other hand $C_1 = 0$ up to numerical errors since the discretization errors are $O(10^{-6})$. Thus we can conclude that $\left|\mathcal{F}[w] - \mathcal{F}[v^l]\right| \sim$ numerical errors. For our current (adaptive) methods, these numerical errors are of the order 10^{-6}.

4.4   Analysis of the lamellar phase of (OK) in two dimensions.

In this section we extend our analysis to a computed lamellar structure on a 2D square torus. We show that a computed lamellar phase is optimal with respect to perturbations restricted to various subspaces of $H^1(\Omega)$. We note that difficulties in arguing optimality over all perturbations are due to symmetries in the domain and may be overcome in other domains such as an asymmetric rectangle. Let $m = 0$, $\gamma = 2.02$ with torus size $4\pi \times 4\pi$. To obtain the candidate minimizer $v^l(\mathbf{x})$, we again run an H^{-1} gradient flow (4.12) on the sinusoidal initial data $v(\mathbf{x}, 0) = \sin(x)\cos(y)$. We run the gradient flow (integration time $T \sim 2000$) to a required tolerance $\epsilon = 8 \times 10^{-10}$. As a result, we obtain a candidate minimizer v^l, shown in Figure 12.

In 2D, a number of symmetries exist in both the functional and in the candidate minimizer v^l, which can be described using the orbit-stabilizer theorem. Let $\mathbf{G}$ denote the symmetry group acting on functions v, that leaves $\mathcal{F}$ invariant. Let $\mathbf{H}$ be the symmetry group that stabilizes the candidate minimize v^l. We then refer to the *symmetry group* of v^l as the orbit-stabilizer quotient group $\mathbf{G}/\mathbf{H}$. Note that the constant state has $\mathbf{H} = \mathbf{G}$ and hence $v^l = m$ has a trivial symmetry group. In 2D, the group $\mathbf{G}$ is generated by the following subgroups:

- The discrete dihedral group of order 4 generated by a $\pi/2$-rotation and a flip.
- The continuous group of translations.
- Inversion $v(\mathbf{x}) \to -v(\mathbf{x})$.

The computed lamellar structure v^l (Figure 12) has a stabilizer group $\mathbf{H}$ consisting of

- A discrete flip along the line $y = x$.
- Rotations of π.
- Arbitrary translations along the direction $(1, -1)$.

30

- Discrete translations along $(1,1)$ with length $\sqrt{2}\pi$.
- An inversion $v \to -v$, followed by a discrete translation along $(1,1)$ with length $\pi/\sqrt{2}$.

One immediate difference to 1D is that the orbits of $v^l(\mathbf{x})$ generate a symmetry group $\mathbf{G}/\mathbf{H}$ consisting of two tori. These tori may be parameterized by

$$v^l(x+s, y+s), \qquad v^l(-x-s, x+s) \quad \text{for } s \in \mathbb{R}.$$

In light of the above symmetries, we introduce the following vectors [8]

$$e_1 := \partial_x v^l(\mathbf{x}), \quad e_2 := \partial_x v^l(4\pi - x, y), \quad e_3 := v^l(4\pi - x, y), \quad e_4 := v^l(\mathbf{x}),$$

and subspaces of $\mathcal{H}$

$$\mathcal{Z} := \{u \in \mathcal{H} \mid \langle u, e_j \rangle = 0, j = 1 \dots 4\} \qquad \mathcal{U} := span\{e_1, e_2, e_3\}, \qquad \mathcal{V} := span\{e_4\},$$

so that $\mathcal{H} = \mathcal{U} \bigoplus \mathcal{V} \bigoplus \mathcal{Z}$. We now argue that v^l is nearly optimal when restricting search directions f to any one of the subspaces $\mathcal{U}$, $\mathcal{V}$ or $\mathcal{Z}$.

As before we may, without loss of generality, restrict search directions f so that $\langle f, e_1 \rangle = 0$. Unfortunately the argument used to show that $\langle f, e_1 \rangle = 0$ will not simultaneously work for e_2, e_3 and e_4. Suppose $w(x) = A\sin(x-y) + B\sin(x+y) + C\cos(x-y) + D\cos(x+y)$ is the global minimizer and $v(x) = a\sin(x-y)$ is the candidate minimizer. Then one can shift $w(x)$ so that $w(x') = A'\sin(x-y) + B'\sin(x+y)$. However, no shift or flip will make $(w-v) \perp \sin(x+y)$ and simultaneously $\perp \cos(x+y)$.

The subspace $\mathcal{Z}$: Numerically, we find the smallest eigenvalues of $B - 2(v^l)^2$ over $\mathcal{H}$ to be

$$-0.0066 \quad -0.0033 \quad -0.0033 \quad 0.0000 \quad 0.0023,$$

the latter with a degeneracy of 4. The corresponding eigenvectors (Figure 13) have a large overlap with v_x^l (smallest eigenvalue), $v^l(4\pi - x, y)$, and $v_x^l(4\pi - x, y)$ with the eigenspace associated with eigenvalue -0.0033, while v^l has eigenvalue 0. Note that all the eigenvectors corresponding to eigenvalues below 0 are associated with symmetries of the energy, while higher eigenvectors (Figure 14) are not related in a simple fashion.

We now argue that our computed v^l is very close to being a global minimizer **over** perturbations $f \in \mathcal{Z}$. Indeed repeating the steps presented in Section 4.3, we find

$$\delta_{v^l}\mathcal{F}_1[f] \geq -\epsilon \|f\|_{H^{-1}} + \langle f, (B - 2(v^l)^2)f \rangle, \qquad \forall f \in \mathcal{H}.$$

Restricting $f \in \mathcal{Z}$, we solve for the smallest constrained eigenvalue to the operator $B - 2(v^l)^2$ and find $C_1 = 0.0023$. Consequently we have

$$
\begin{aligned}
\delta_{v^l}\mathcal{F}_1[f] &\geq -\epsilon \|f\|_{H^{-1}} + C_1\|f\|^2, \qquad \forall f \in \mathcal{Z} \\
&\geq -\epsilon \|f\|_{H^{-1}} + \frac{C_1}{16}\|f\|_{H^{-1}}^2 \\
&\geq -\frac{4\epsilon^2}{C_1} > -4 \times 10^{-16}
\end{aligned}
$$

---

[8]For simplicity, when defining e_1 and e_2 we take the derivatives in the $(1,0)$, or x direction. Due to the fact that v^l is a lamellae, the derivative along $(1,0)$ is proportional to the derivative along the direction $(1,1)$.
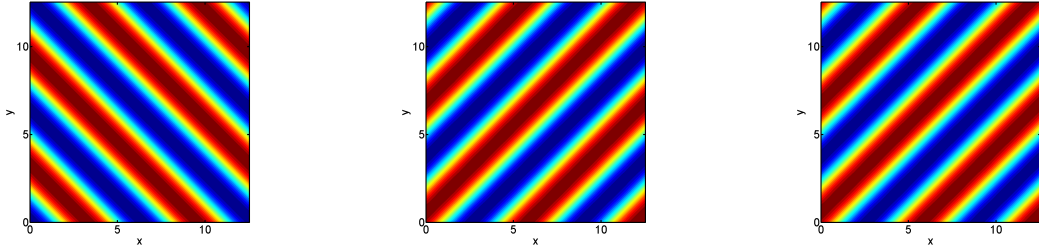
Figure 13: Plot of the first three eigenvectors of the operator $B - 2(v^l)^2$, corresponding to the eigenvalues below 0. The plot of v^l corresponding to eigenvalue 0 is given in Figure 12. The eigenvectors very closely resemble the symmetry transformations e_1, e_2, e_3.
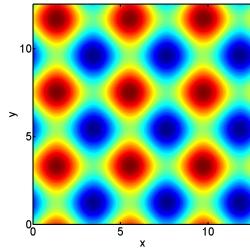

Figure 14: Plot of e_5, the eigenvector corresponding to the first eigenvalue above 0.

where in the middle line we used the Poincaré-type inequality[9] $||f|| \geq (1/4)||f||_{H^{-1}}$, and in the last line, we optimized over $||f||_{H^{-1}}$. We arrive at the following result. Let w be the exact global minimizer over perturbations $f \in \mathcal{Z}$, then

$$0 \leq \mathcal{F}_1[v^l] - \mathcal{F}_1[w] < 4 \times 10^{-16}.$$

The subspace $\mathcal{U}$: We make a general remark regarding lamellae functions. Suppose v^l is a mean zero ($\langle v^l \rangle = 0$) lamellae function oriented along the vector $\mathbf{n} = \frac{1}{\sqrt{2}}(-1, 1)$. Namely $\mathbf{n} \cdot \nabla v^l = 0$. Let f be any lamellae function in the perpendicular direction along $\mathbf{n}_\perp = \frac{1}{\sqrt{2}}(1, 1)$. Then f^3 is also lamellae along $\mathbf{n}_\perp$ and hence the integral $\langle v^l f^3 \rangle = 0$ by virtue of the fact that $\langle v^l \rangle = 0$. Let f be any function such that $\mathbf{n}_\perp \cdot \nabla f = 0$. Then the energy in such directions is always positive

$$\delta_{v^l} \mathcal{F}_1[f] = b(f, f) + \langle v^l f^3 \rangle + \frac{1}{4} \langle f^4 \rangle \tag{4.16}$$

$$= b(f, f) + \frac{1}{4} \langle f^4 \rangle \tag{4.17}$$

$$\geq 0 \tag{4.18}$$

Now suppose w is a global minimizer with $f = w - v^l \in \mathcal{U}$. Then translating f so that $\langle f, e_1 \rangle = 0$, we have that $f = ae_2 + be_3$ for some constants a, b. It follows that f is a lamellae

---

[9]Here 1/4 is the Poincaré constant for the torus with length 4π.

function along $\mathbf{n}_\perp$ and hence $\mathcal{F}_1[w] \geq \mathcal{F}_1[v^l]$ has a higher energy.

The subspace $\mathcal{V}$: We have that $\pm v^l$ solves the Euler-Lagrange equations (to a tolerance ϵ), with a positive semi-definite second variation $b(f, f) \geq 0$. Since the energy $\mathcal{F}_1[\lambda v^l]$ is a quartic in λ, there are only 2 local minima found at $\lambda = \pm 1$. Hence v^l is almost optimal in $\mathcal{V}$.

Unfortunately, the non-convexity of $\mathcal{F}_1$ implies that we could still lower the energy by taking directions which are linear combinations of elements of $\mathcal{Z}$ and suitable combinations of $e_1 \ldots e_4$. Ideally, we would like a lower bound $Q[f]$ for all $f \in \mathcal{H}$:

$$\delta_{v^l} \mathcal{F}_1[f] \quad \geq \quad Q(f, f)$$

For example, if $f = g(x) + h(x)$ with $g \in \mathcal{V}$ and $h \in \mathcal{Z}$, we have

$$\delta_{v^l} \mathcal{F}_1[g + h] \quad \geq \quad Q_1[g] + Q_2[h] + \text{ cross terms in } g \text{ and } h,$$

for positive $Q_1 \geq 0$ and positive-definite Q_2. It is not clear at this time how to use the structure of the energy to control these cross terms.

Thus at this stage, we have computed a lamellar structure v^l for which we can conclude: The computed structure is close (up to numerical error) to being a global minimizer on the infinite dimensional subspace $m + \mathcal{Z}$. If it is not close to the global minimizer over the entire space $m + \mathcal{H}$, then the difference between it and a global minimizer must have a non-zero component in both $\mathcal{U} \bigoplus \mathcal{V}$ and $\mathcal{Z}$. Noting that $e_1 \ldots e_4$ are directly linked to symmetry transformations of v^l (cf. Figure 13), these conclusions provide some support that v^l is indeed close to a global minimizer over all of $m + \mathcal{H}$.

4.5 Analysis of the lamellar phase of (OK) on an aymmetric torus.

In light of the discrete flip symmetries on the square torus, we now consider an asymmetric torus. In breaking the asymmetric flip symmetry about the line $y = x$, the symmetry group $\mathbf{G}$ that leaves $\mathcal{F}$ invariant is reduced while the stabilizer $\mathbf{H}$ for a lamellar phase stays the same. In this setting, we provide numerical evidence that a lamellar phase is optimal for certain aspect ratios and parameters γ. This optimality is not surprising as in Section 5, we will use our first lower bound to prove, for suitable aspect ratios, the optimality of a lamellar phase. To this end, we fix $L_x = 4\pi$ as before, $\gamma = 2.15$ but vary $L_y > 0$. For each L_y, we compute the candidate minimizer, and using the algorithm in appendix A, we compute the constrained minimizer to the eigenvalue problem (4.14). We find that for values of $L_y < 3.82$, the smallest constrained eigenvalue λ_1 is zero up to numerical errors. For $L_y > 3.82$, the eigenvalue drops below zero.

Remark 4 (Two Remarks on the Choice of Parameters and the Use of the First Lower bound). (i) For the lamellar states of the previous three subsections, we used param-
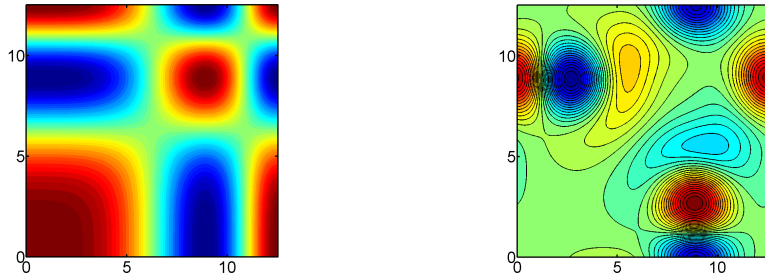
Figure 15: Left: shows the irregular potential (4.19). Right: candidate minimizer v for $m = 0$ and $\gamma = 1.25$. Here v satisfies the Euler-Lagrange equation with an H^{-1} error of $\sim 2 \times 10^{-5}$.

eters which were close to the ODT. As γ becomes large the energy landscape becomes very flat[10] (cf. Section 6).

(ii) One could also pursue the analysis of the last subsections using the improved second quadratic bound which uses the inner product induced by b to obtain a tighter lower bound. To do so would require working on a subspace orthogonal to the null directions of b to enforce its positive definiteness on the appropriate subspace. Hence this strategy is worth pursuing only once we have a better treatment/understanding of the role of symmetries.

4.6 Analysis of non-constant state for (OK) with a spatially non-symmetric potential.

In this subsection, we examine candidate minimizers for the (**OK**) functional with the addition of a spatially dependent potential term $V(\mathbf{x})$ which breaks the symmetries in the domain. We consider the modified functional

$$(\textbf{OK-V}) \qquad \mathcal{F}_3[u] := \int_\Omega \frac{1}{2}\gamma^{-2}|\nabla u|^2 + \frac{1}{2}|\nabla \Delta^{-1}(u - m)|^2 + \frac{1}{4}(1 - u^2)^2 + \frac{1}{2}V(\mathbf{x})(u - m)^2 \, d\mathbf{x}.$$

If $V(\mathbf{x})$ is asymmetric in space, then the functional (**OK-V**) may admit a unique non-constant $v \neq m$ global minimizer. Since there are a wide variety of potentials one could take, we choose one (somewhat arbitrarily) that varies smoothly in space and shares the same periodicity as the domain Ω.

$$V(\mathbf{x}) = \cos\left(2\pi \frac{x^2}{D^2}\right) \cos\left(2\pi \frac{y^2}{D^2}\right) - V_m \quad \text{where} \quad V_m = \fint_\Omega \cos\left(2\pi \frac{x^2}{D^2}\right) \cos\left(2\pi \frac{y^2}{D^2}\right) \, d\mathbf{x}. \tag{4.19}$$

---

[10]We refer to an energy landscape of a functional $\mathcal{F}$ in the vicinity of a local minimize v as flat, if the associated $b(f, f)$ has an eigenvalue $\epsilon \ll 1$ with eigenvector f_ϵ (with $||f_\epsilon|| = 1$). These directions f_ϵ need not be related to symmetries of v. We observe that as one either increases the domain Ω or increases γ in (**OK**), i) the number of small eigenvalues ϵ of $b(f, f)$ increase, and ii) the amplitude of the small eigenvalues also decrease. Hence, in this respect we say (**OK**) becomes increasingly flat.
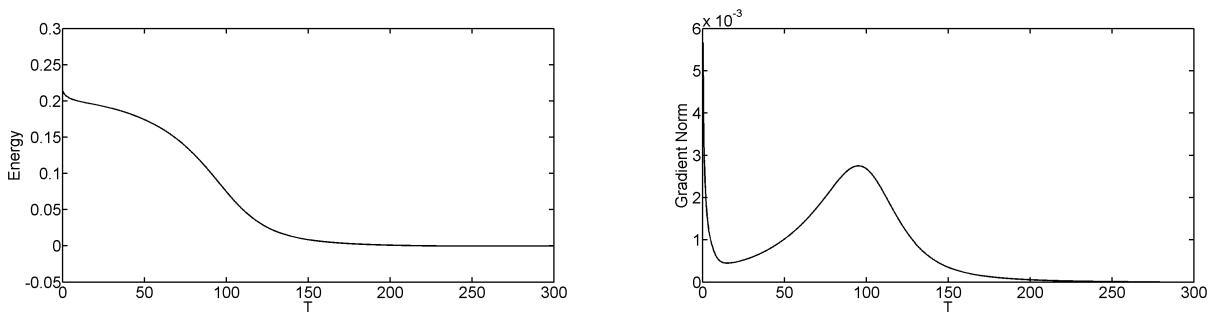
Figure 16: Evolution of energy (left) and the H^{-1} gradient (right) for a gradient flow of (**OKV**) with random initial data. Here $m = 0$ and $\gamma = 1.25$. Note that the evolution implies a non-convex energy landscape.

We now apply our approach to examine candidate minimizers for (**OK-V**) near the ODT curve. We take the domain size $L_x = L_y = 4\pi$ and $m = 0$. For $m = 0$ and the associated domain, the constant solution $v = m = 0$ becomes unstable for $\gamma \approx 1.23$. Choosing the value $\gamma = 1.25$ and a grid of 256×256, we run a gradient flow of (**OK-V**) with random initial data to obtain our candidate minimizer v. Figure 15 shows the candidate minimizer, while Figure 16 shows the evolution of the energy and associated gradient during the gradient flow. We note that although the gradient does not decrease monotonically, for the current parameters we could not find other distinct local minima suggesting that perhaps v is also the only local minimum. Once we obtain a candidate minimizer v, we then compute the two lower bound coefficients C_j for $j = 1, 2$ to determine if they are non-negative. We note that in the calculations $\langle V f^2 \rangle$ is directly added into the bilinear form $b(f, f)$ and $2V(\mathbf{x})$ is added to the associated operator B.

Since $\mathcal{F}_3$ and $m = 0$ is invariant under $v \to -v$, any convex (quadratic) lower bound must be optimal in the direction $f = -v$. Hence, any lower bound coefficient $C_j \leq 0$ for $j = 1, 2$. We seek to show that for the current parameters γ, the lower bound coefficient is optimal ($C_j = 0$).

For our candidate v at $\gamma = 1.25$, we compute the first 3 eigenvalues of (4.9) as

$$-0.0001 \qquad 0.0149 \qquad 0.025$$

yielding $C_1 = -0.0001$. As expected, the first eigenvalue is (up to numerical errors) 0 and corresponds to the function $\psi = v$ satisfying (4.10). Furthermore, a convergence study, not included here, shows that the smallest eigenvalue decreases in magnitude as one refines the mesh, verifying that the smallest eigenvalue is 0.

Meanwhile the second eigenvalue $\lambda_2 = 0.0149$ is bounded away from 0 implying that v is the global minimizer[11]. We also compute the lower bound coefficient $C_2 = -0.0001$.

We continue the procedure of verifying non-constant candidate minimizers for $\gamma \geq 1.25$. Let v_γ parameterize the candidate minimizer for different γ. To obtain v_γ, we start with $\gamma = 1.25$ and $v_{1.25}$ as initial data. We then gradually (adiabatically) increase γ which continuously changes the energy landscape of (**OK-V**). As the landscape changes, we constantly recompute

---

[11]Although the second eigenvalue 0.0149 is close to 0, the values are accurate to approximately 10^{-4}.
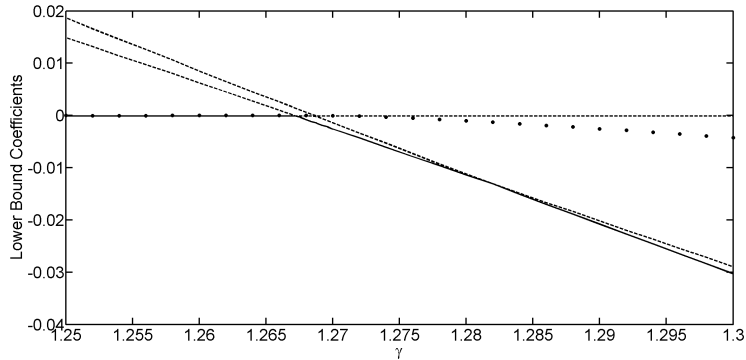
35

Figure 17: Coefficients of the quadratic lower bounds: solid line represents the coefficient using the first lower bound while the dotted line represents the second lower bound. The solid curve $(C_1 = \lambda_1)$ is only piecewise smooth with kinks that arise from eigenvalue collisions. In addition we also plot the second and third eigenvalues λ_2 and λ_3, as dashed lines to show how they relate to the smallest eigenvalue of (4.9) λ_1. Note that there is always an eigenvalue $\lambda = 0$. The values numerically support that v is the global minimizer for $\gamma < 1.269$. For $\gamma > 1.269$, two eigenvalues drop below 0.

the candidate minimizer using a gradient flow to obtain v_γ. For each pair γ and v_γ we then compute the first 3 eigenvalues of the (4.9), as well as the lower bound coefficient C_2 and plot them in Figure (17). Here the plot shows that the second and third eigenvalue collide with $\lambda = 0$ around the parameter $\gamma \sim 1.269$. Hence, for values $\gamma < 1.269$, we have up to numerical errors, verification that our computed v_γ is the global minimizer to (**OK-V**), while for $\gamma > 1.269$, the lower bound contains negative definite directions.

5 A Rigorous Connection Between 1D and 2D Minimizers of (OK)

In this section we focus on (**OK**) on a rectangular torus of side lengths L_x by L_y. We use our first convex lower bound to rigorously prove that for certain values of γ, L_x, and L_y, any global minimizer $v(x)$ for the 1D problem on the torus $[0, L_x]$, is automatically a global minimizer on the 2D torus. An asymptotic result, similar in spirit, for a sharp interface version of (**OK**) was recently presented in [17]. However, we remark that our approach is elementary and yields exact values for γ and L_y. We first prove that in a certain explicit regime for L_y and γ, any global minimizer on the 2D torus must be a function of x only.

Theorem 5.1. *Fix $L_x > 0$, $\gamma > 0$ and let $L_y > 0$ be such that $L_y \leq \frac{2\pi}{\gamma}$. Let $v(x, y)$ be a global minimizer for $\mathcal{F}_1$ on the two dimensional torus $\Omega = [0, L_x] \times [0, L_y]$. Then $v(x, y)$ is a function only of x, i.e. $v(x, y) = v(x)$.*

Proof. Our proof requires a simple result regarding the criticality of 1D functions with respect to y-dependent perturbations. Specifically, let $w(x) \in H^1(\Omega)$ be any function depending only

on x (not necessarily a critical point of the functional $\mathcal{F}_1$), and let $f(x, y) \in \mathcal{H}$ (i.e., a function in $H^1(\Omega)$ with average 0) such that $\int_0^{L_y} f(x, y) \, dy = 0$ holds for a.e. $x \in [0, L_x]$. We claim the first variation in f vanishes, i.e.,

$$
\begin{aligned}
2 \, a(w, f) &+ \int_\Omega w(w^2 - 1) f \, d\mathbf{x} \\
&= \int_\Omega \gamma^{-2} (\nabla w) \cdot (\nabla f) + (-w + w^3) f \, d\mathbf{x} \; + \; \int_\Omega \left(\nabla (-\Delta)^{-1} (w - m) \right) \cdot \left(\nabla (-\Delta)^{-1} f \right) d\mathbf{x} \\
&= 0
\end{aligned}
\tag{5.1}
$$

This follows by using Fubini's theorem and integrating over the y variable first to show that all the integrals above (5.1) vanish separately. To this end, we start with the non-local term. First note that $W := (-\Delta)^{-1}(w(x) - m)$ depends only on x. Now let $F := (-\Delta)^{-1} f$. Assume for the moment that $f \in C^\infty(\Omega)$, hence, by elliptic regularity $F \in C^\infty(\Omega)$. Then

$$
-\partial_{xx} F - \partial_{yy} F = f \quad \Longrightarrow \quad -\partial_{xx} \left(\int_0^{L_y} F \, dy \right) - \int_0^{L_y} \partial_{yy} F \, dy = \int_0^{L_y} f \, dy = 0.
$$

Hence

$$
-\partial_{xx} \left(\int_0^{L_y} F \, dy \right) = 0.
$$

Since F is continuous on the torus, we have

$$
\partial_x \left(\int_0^{L_y} F(x, y) \, dy \right) = 0.
$$

The non-local term reduces to

$$
\begin{aligned}
\int_\Omega (\partial_x W)(\partial_x F) \, d\mathbf{x} &= \int_0^{L_x} (\partial_x W) \left(\int_0^{L_y} \partial_x F \, dy \right) dx \\
&= \int_0^{L_x} (\partial_x W) \, \partial_x \left(\int_0^{L_y} F \, dy \right) dx \\
&= 0.
\end{aligned}
$$

This property extends to $f \in H^1(\Omega)$ by a density argument via a sequence $f_n \in C^\infty(\Omega)$ which converges in $H^1(\Omega)$ to f, in which case the associated potentials $F_n := (-\Delta)^{-1} f_n$ also converge to F in $H^1(\Omega)$.

For the other terms we find that, for $f \in C^\infty(\Omega)$,

$$
\begin{aligned}
\int_\Omega \gamma^{-2} (\nabla w) \cdot (\nabla f) \, d\mathbf{x} &= \int_0^{L_x} \gamma^{-2} (\partial_x w) \left(\int_0^{L_y} (\partial_x f) \, dy \right) dx = 0, \\
\int_\Omega (-w + w^3) f \, d\mathbf{x} &= \int_0^{L_x} (-w + w^3) \left(\int_0^{L_y} f \, dy \right) dx = 0.
\end{aligned}
$$

Again, we use a density argument to extend to $f \in H^1(\Omega)$. This proves (5.1).

37

Suppose now that $v(x, y)$ is a global minimizer to $\mathcal{F}_1$. We show that the projection of $v(x, y)$ onto a 1D pattern has lower energy. Let $f(x, y) \in H^1(\Omega)$ be such that

$$v(x, y) = w(x) + f(x, y) \qquad \text{where} \qquad w(x) = \frac{1}{L_y} \int_0^{L_y} v(x, y) \, \mathrm{d}y.$$

By the mass constraint, we have

$$\frac{1}{L_x} \int_0^{L_x} w(x) \, \mathrm{d}x = m \qquad \text{and} \qquad \int_0^{L_y} f(x, y) \, \mathrm{d}y = 0 \text{ for a.e. } x \in [0, L_x].$$

Now consider the energy difference between the global minimizer $v(x, y)$ and its projection $w(x)$:

$$
\begin{aligned}
\mathcal{F}_1[v] - \mathcal{F}_1[w] &= \mathcal{F}_1[w + f] - \mathcal{F}_1[w] \\
&= a(f, f) + \int_\Omega \frac{3}{2} w^2 f^2 - \frac{1}{2} f^2 + w f^3 + \frac{1}{4} f^4 \, \mathrm{d}x \, \mathrm{d}y \\
&\geq a(f, f) + \int_\Omega \frac{1}{2} w^2 f^2 - \frac{1}{2} f^2 \\
&= \int_\Omega \frac{\gamma^{-2}}{2} |\nabla f|^2 + \frac{1}{2} |\nabla(-\Delta)^{-1} f|^2 - \frac{1}{2} f^2 + \frac{1}{2} w^2 f^2 \, \mathrm{d}x \, \mathrm{d}y \\
&\geq \int_\Omega \frac{\gamma^{-2}}{2} (\partial_y f)^2 - \frac{1}{2} f^2 \, \mathrm{d}x \, \mathrm{d}y \\
&\geq \left(\left(\frac{2\pi}{L_y \gamma} \right)^2 - 1 \right) \frac{1}{2} \int_\Omega f^2 \, \mathrm{d}x \, \mathrm{d}y.
\end{aligned}
$$

To pass to the second line, we made use of (5.1). To pass to the third line, we used the analogous lower bound (our first lower bound) as in (4.8). To pass to the last line, we used the Poincaré inequality on f for each slice as a function of y. Hence if $L_y \leq \frac{2\pi}{\gamma}$, then $\mathcal{F}_1[w] \leq \mathcal{F}_1[v]$. Since by definition of v we have $\mathcal{F}_1[w] \geq \mathcal{F}_1[v]$, it follows that $f \equiv 0$ a.e. and $v(x, y) = w(x)$ a.e. $\qquad \square$

Since for the parameters in Theorem 5.1 the global minimizer to $\mathcal{F}_1$ in 2D, which depends only on x, is also the global minimizer to $\mathcal{F}_1$ in one dimension $[0, L_x]$, we have the following immediate corollary:

Corollary 5.2. *For the parameters in Theorem* 5.1, *any global minimizer to the* 1D *problem on* Ω *is also a global minimizer to the* 2D *problem.*

Note that while we stated and proved Theorem 5.1 on the 2D torus, the same is true on the n-dimensional torus with L_y being the side length of all sides except that corresponding to x. A similar argument would also yield, for instance, that if $v(x, y)$ is a global minimizer for $\mathcal{F}_1$ on the 2D torus of size $L_x \times L_y$, then for $L_z \leq \frac{2\pi}{\gamma}$, $v(x, y, z) = v(x, y)$ is the global minimizer on the 3D torus of size $L_x \times L_y \times L_z$. In a similar spirit, if $\max\{L_x, L_y\} \leq \frac{2\pi}{\gamma}$, then the global minimizer is the constant state $v = m$.

The previous theorem makes no use of the structure of $v(x)$. On the other hand combining the theorem with previous work on the 1D **(OK)** problem, we can now rigorously prove that for certain values of γ, L_x, and L_y, a lamellar state is a global minimizer. Indeed, on the 1D torus it has been shown in [18, 25] (for the case $m = 0$) and in [21] for general m, that for $\gamma > \gamma_c$, a periodic structure $v(x)$ must be a global minimizer. In fact, their results prove more: Any global minimizer for $\gamma > \gamma_c$ (in fact, even a suitable local minimizer) must be periodic. See, for example, Theorem 1.1 of Ren & Wei in [21]. Theorem 5.1 implies that there is a threshold for L_y/L_x, in terms of γ_c, below which the periodic lamellar structure $v(x)$ is a global minimizer on the 2D torus. In other words, this proves the existence of periodic lamellar global minimizers to **(OK)** in higher dimensions. Precisely, we have the following result:

Corollary 5.3. *Consider minimization of* **(OK)** *for any $m \in (-1, 1)$ on an n-dimensional flat torus with one fixed side length, L_0 and $n - 1$ side lengths L. There exist values of γ and L such that a periodic lamellar structure, i.e., a periodic structure depending only on one variable, is a global minimizer.*

6 Summary and Discussion

For a class of non-convex energy functionals, we have presented a simple strategy to verify whether or not a given metastable state is a global minimizer. In addition to the Ohta-Kawasaki, Phase-Field Crystal and other Swift-Hohenberg-type functionals, this class includes the simpler classical Ginzburg-Landau and Cahn-Hilliard functionals. Our method was based upon finding a global quadratic lower bound for the excess energy about a critical point. We gave two simple ways to find such lower bounds.

In Section 3 we considered the simplest metastable state: the constant state. We showed the the second approach for a lower bound worked particularly well; indeed for both the Ohta-Kawasaki and Phase-Field Crystal energies, it gave a good estimate for the actual true order-disorder curve in phase space. However, we also note that one might further improve the current ODT estimate by analyzing the structure of the ratio in (3.7). Note that the method was numerically robust and independent of domain geometry or dimension.

In Section 4 we applied our methodology to the verification of non-constant candidate minimizers $v \not\equiv m$. Here one must deal with certain symmetry invariants of the energy, and appropriately constrain the class of perturbation methods. Focusing on the Ohta-Kawasaki energy and our first lower bound, we showed that this can be successfully done on the 1D torus and on certain asymmetric 2D tori. In these cases, we computed a lamellar state for which we were able to numerically verify was close to being globally optimal. On the symmetric 2D torus, however, the additional symmetry invariants led us to only a partial answer. Here we were able to argue global optimality of a computed lamellar state only with respect to perturbations which were orthogonal to four eigenfunctions directly tied to symmetries of v^l.

In Section 5 we used our first lower bound to prove that global minimizers to the Ohta-Kawasaki energy on the 1D torus are also global minimizers on certain asymmetric higher-dimensional tori. Combining this result with previous work on the 1D torus, we were able to

prove the existence of periodic, lamellar global minimizers to the Ohta-Kawasaki energy on certain higher-dimensional domains.

We conclude with a few observations. The addition of symmetries in the energy functionals lead to degenerate global minimizers. As a general observation, using a lower bound functional to verify that a state is a global minimizer requires either: i) removing search directions of symmetry or ii) requiring that the lower bound be optimal (flat) in any direction of symmetry.

One difficulty when dealing with the (**OK**) functional is that the energy landscape becomes very flat as γ becomes large. Specifically, if v is a global minimizer of $\mathcal{F}_1$ and $b(f, f) \geq 0$ is the second variation about v, then as γ becomes large, $b(f, f)$ contains many directions f along which $b(f, f)$ is small. Furthermore, as the domain size becomes large, the addition of the long wavelengths can introduce more directions where $b(f, f)$ becomes small. Indeed, one might wonder as to why in Sections 4.3-4.6 we chose a value for γ close to 2 (i.e., close to the ODT curve). Here the number of eigenvalues less that 0 to the operator $B - 2v^2$ increases with γ. By choosing values of γ close to 2 we restrict the number of eigenvalues less than 0 to 3. The eigenvectors appear both related to the smallest eigenvalues of B (without the potential v^2) as well as the symmetries of the domain. For large values of γ many more eigenvalues appear which are less than 0. In addition, although many of the eigenvectors appear to be associated with symmetries of the domain, many do not. Hence, the approach presented here, using a quadratic lower bound and accounting for symmetries, is restricted to small values of γ. For example, we also examined the operator $B - 2v^2$ using the (far from the ODT) parameters $\gamma = 10$ and $m = 0.25$ mentioned in Figure 1. We did so about both the hexagonal and lamellae states where we believe the hexagonal structure is the true ground state. In both cases several eigenfunctions appeared to be related to translations of the hexagonal or lamellae state. However, in both cases, we also found eigenfunctions with additional structures. Since the quadratic functional containing the operator $B - 2v^2$ is only a lower bound to the energy, there is no a priori reason that eigenfunctions with eigenvalues less that 0 should represent physically lower energy states – but only rather that they may suggest such states.

A   Appendix: Solving the Constrained Eigenvalue Problem

We seek to compute the minimizer of $\langle \psi, (B - 2v^2)\psi \rangle$ subject to

$$
\begin{aligned}
\langle \psi^2 \rangle &= 1 \\
\langle \psi, \partial_x v(\mathbf{x}) \rangle &= 0
\end{aligned}
$$

Due to the large matrices involved, it is more efficient to first ignore the orthogonality constraint and build a low rank approximation to $(B - 2v^2)$ over the entire unconstrained space.

Once the low rank approximation is built, we then project out the appropriate orthogonality constraints and solve for the minimizer of $(B - 2v^2)$.

1. Build numerical finite difference operators:

$$\begin{aligned} \mathbf{L} &= \gamma^{-2}(\Delta^2) - (\Delta)(3v^2(\mathbf{x}) - 1) + I, \\ \mathbf{D} &= (-\Delta) \end{aligned}$$

2. Use MATLABs eigenvalue function

$$[\mathbf{Q} \ \mathbf{\Lambda}] = eigs(\mathbf{L}, \ \mathbf{D}, \ k, \ 'sm')$$

to compute the first k eigenvectors and values to the eigenvalue problem:

$$\mathbf{L}\mathbf{q}_j = \lambda_j \mathbf{D}\mathbf{q}_j \quad j = 1 \dots k$$

Here $\mathbf{Q} = [\mathbf{q}_1 \ \mathbf{q}_2 \ \dots \ \mathbf{q}_k]$, while $\mathbf{\Lambda} = \text{diag}[\lambda_1 \ \lambda_2 \dots \lambda_k]$.

3. Orthonormalize $\mathbf{q}$ with respect to the standard ℓ^2 inner product (if they are not orthonormal already).

We now have the numerical representation for operator $(B - 2v^2)$ as follows:

$$\begin{aligned} (B - 2v^2) &\approx \mathbf{D}^{-1}\mathbf{L} \\ &= \mathbf{Q}\mathbf{\Lambda}\mathbf{Q}^T + \mathbf{R} \end{aligned}$$

where $\mathbf{R}^T = \mathbf{R}$ is a remainder term. Choose k large enough so that $\mathbf{R}$ is a positive-definite matrix. Hence for any discrete vector ψ, we then have:

$$\psi^T \mathbf{D}^{-1}\mathbf{L}\psi \geq \psi^T \mathbf{Q}\mathbf{\Lambda}\mathbf{Q}^T\psi \quad \text{for all } \psi$$

Finally, we minimize $\psi^T \mathbf{Q}\mathbf{\Lambda}\mathbf{Q}^T\psi$ over the subspace $\psi^T \mathbf{e}_1 = 0$ with $||\psi|| = 1$, where $\mathbf{e}_1 \approx \frac{\partial v}{\partial x}$ is the discrete vector for $\frac{\partial v}{\partial x}$. The above problem can be solved using straightforward methods as k will generally be small.

References

[1] S. ADAMS, N. DIRR, M. PELETIER, AND J. ZIMMER, *From a Large-deviations Principle to the Wasserstein Gradient Flow: a New Micro-macro Passage.*, Comm. Math. Phys., 307 (2011), pp. 791–815.

[2] M. BECK, J. KNOBLOCH, D. LLOYD, B. SANDSTEDE, AND T. WAGENKNECHT, *Snakes, Ladders, and Isolas of Localized Patterns*, SIAM J. Math. Anal., 41 (2009), pp. 936–972.

[3] J. CAHN AND J. HILLIARD, *Free Energy of a Nonuniform System I. Interfacial Free Energy*, J. Chem. Phys., 28 (1958), pp. 258–267.

[4] R. Choksi, *On Global Minimizers for a Variational Problem with Long-range Interactions*, Quart. Appl. Math., 70-3 (2012), pp. 517–537.

[5] R. Choksi, M. Maras, and J. Williams, *2D Phase Diagram for Minimizers of a Cahn-Hilliard Functional with Long-range Interactions*, SIAM J. Appl. Dyn. Syst., 10 (2011), pp. 344–1362.

[6] R. Choksi, M. A. Peletier, and J. F. Williams, *On the Phase Diagram for Microphase Separation of Diblock Copolymers: an Approach via a Nonlocal Cahn-Hilliard Functional.*, SIAM J. Applied Math., 69-6 (2009), pp. 1712–1738.

[7] M. Cicalese, E. Spadaro, and Z. C.I., *Asymptotic Analysis of a Second-order Singular Perturbation Model for Phase Transitions.*, Calc. Var., 41 (2011), pp. 127–150.

[8] B. Coleman, M. Marcus, and V. Mizel, *On the Thermodynamics of Periodic Phases* , Arch. Rational Mech. Anal., 117 (1992), pp. 321–347.

[9] M. Cross and P. Hohenberg, *Pattern Formation Outside of Equilibrium*, Reviews of Modern Physics, 65 (1993), pp. 851–1111.

[10] R. Desai and R. Kapral, *Dynamics of Self-Organized and Self-Assembled Structures*, Cambridge University Press, 2009.

[11] G. Di Fratta, J. Robbins, V. Slastikov, and A. Zarnescu, *Profiles of Point Defects in Two Dimensions in Landau-de Gennes Theory*, preprint, (2014).

[12] K. R. Elder, M. Katakowski, M. Haataja, and M. Grant, *Modeling Elasticity in Crystal Growth*, Phys. Rev. Lett., 88 (2002), p. 245701.

[13] H. Emmerich, H. Löwen, R. Wittkowski, T. Gruhn, G. Tóth, G. Tegzec, and L. Grnsy, *Phase-field-crystal Models for Condensed Matter Dynamics on Atomic Length and Diffusive Time Scales: an Overview*, Advances in Physics, 61 (2012), pp. 665–743.

[14] K. Glasner, *Spatially Locallized Structures in Diblock Copolymer Mixtures*, SIAM J. Appl. Math, 70 (2010).

[15] R. Jordan, D. Kinderlehrer, and F. Otto, *The Variational Formulation of the Fokker-Planck Equation*, SIAM J. Math. Anal., 29 (1998), pp. 1–17.

[16] R. Kohn, *Energy-driven Pattern Formation*, Proceedings of the International Congress of Mathematicians, I (2007), pp. 359–383.

[17] M. Morini and P. Sternberg, *Cascade of Minimizers for a Nonlocal Isoperimetric Problem on Thin Domains*, submitted preprint, (2013).

[18] S. Müller, *Singular Perturbations as a Selection Criterion for Periodic Minimizing Sequences*, Calc. Var., 1 (1993), pp. 169–204.

[19] R. Netz, D. Andelman, and M. Schick, *Interfaces of Modulated Phases*, Phys. Rev. Lett., 79 (1997), p. 1058.

[20] T. Ohta and K. Kawasaki, *Equilibrium Morphology of Block Copolymer Melts*, Macromolecules, 19 (1986), pp. 2621–2632.

[21] X. Ren and J. Wei, *On Energy Minimizers of the Diblock Copolymer Problem*, Interfaces Free Boundaries, 5 (2003), pp. 193–238.

[22] M. Seul and D. Andelman, *Domain Shapes and Patterns: The Phenomenology of Modulated Phases*, Science, 267 (1995), p. 467.

[23] J. Swift and P. Hohenberg, *Hydrodynamic Fluctuations at the Convective Instability*, Phys. Rev. A, 15 (1977), pp. 319–328.

[24] S. Villain-Guillot and D. Andelman, *The Lamellar-Disorder Interface : One-Dimensional Modulated Profiles*, Eur. Phys. J., B (1998), pp. 95–101.

[25] N. Yip, *Structure of Stable Solutions of a One-dimensional Variational Problem*, ESAIM: Control, Optimisation and Calculus of Variations, 12-4 (2006), pp. 721–751.